American Society for Neurochemistry

ASN Neuro
Volume 13: 1–18

DOI: 10.1177/17590914211044882
journals.sagepub.com/home/asn
SAGE

Microglial- and Astrocyte-Specific Expression of Purinergic Signaling Components and Inflammatory Mediators in the Rat Hippocampus During Trimethyltin-Induced Neurodegeneration

Milorad Dragić[1], Nataša Mitrović[2], Marija Adžić[1,3], Nadežda Nedeljković[1], and Ivana Grković[2]

Abstract

The present study examined the involvement of purinergic signaling components in the rat model of hippocampal degeneration induced by trimethyltin (TMT) intoxication (8 mg/kg, single intraperitoneal injection), which results in behavioral and neurological dysfunction similar to neurodegenerative disorders. We investigated spatial and temporal patterns of ecto-nucleoside triphosphate diphosphohydrolase 1 (NTPDase1/CD39) and ecto-5′ nucleotidase (eN/CD73) activity, their cell-specific localization, and analyzed gene expression pattern and/or cellular localization of purinoreceptors and proinflammatory mediators associated with reactive glial cells. Our study demonstrated that all Iba1+ cells at the injured area, irrespective of their morphology, upregulated NTPDase1/CD39, while induction of eN/CD73 has been observed at amoeboid Iba1+ cells localized within the hippocampal neuronal layers with pronounced cell death. Marked induction of $P2Y_{12}R$, $P2Y_6R$, and $P2X_4$-messenger RNA at the early stage of TMT-induced neurodegeneration might reflect the functional properties, migration, and chemotaxis of microglia, while induction of $P2X_7R$ at amoeboid cells probably modulates their phagocytic role. Reactive astrocytes expressed adenosine A_1, A_{2A}, and $P2Y_1$ receptors, revealed induction of complement component C3, inducible nitric oxide synthase, nuclear factor-kB, and proinflammatory cytokines at the late stage of TMT-induced neurodegeneration. An increased set of purinergic system components on activated microglia (NTPDase1/CD39, eN/CD73, and $P2X_7$) and astrocytes (A_1R, $A_{2A}R$, and $P2Y_1$), and loss of homeostatic glial and neuronal purinergic pathways ($P2Y_{12}$ and A_1R) may shift purinergic signaling balance toward excitotoxicity and inflammation, thus favoring progression of pathological events. These findings may contribute to a better understanding of the involvement of purinergic signaling components in the progression of neurodegenerative disorders that could be target molecules for the development of novel therapies.

Keywords

astrocyte-derived inflammation, eN/CD73, hippocampal neurodegeneration, microglial polarization, NTPDase1/CD39, purinergic receptors

Received May 19, 2021; Revised August 18, 2021; Accepted for publication August 20, 2021

Introduction

Neurotoxicants, such as trimethyltin (TMT)-chloride, have been reported as risk factors for the development of neurodegenerative disorders (Kotake, 2012; Pompili et al., 2020; Yegambaram et al., 2015). In rats, TMT selectively targets the limbic region, particularly the hippocampus, with a similar pattern as observed in humans and with comparable behavioral alterations (Corvino et al., 2013, 2015; Ferraz da Silva et al., 2017; Geloso et al., 2011; Haga et al., 2002; Lattanzi et al., 2013; Lee et al., 2016; Trabucco et al., 2009). TMT-induced neurodegeneration in rats is characterized by early astrocyte

[1]Department for General Physiology and Biophysics, Faculty of Biology, University of Belgrade, Belgrade, Serbia
[2]Department of Molecular Biology and Endocrinology, VINČA Institute of Nuclear Sciences-National Institute of the Republic of Serbia, University of Belgrade, Belgrade, Serbia
[3]Center for Laser Microscopy, Faculty of Biology, University of Belgrade, Belgrade, Serbia

Corresponding Author:
Ivana Grković, Department of Molecular Biology and Endocrinology, VINČA Institute of Nuclear Sciences - National Institute of the Republic of Serbia, University of Belgrade, Mike Petrovića Alasa 12-14, P.O.Box 522-090 11000 Belgrade, Serbia.
Email: istanojevic@vin.bg.ac.rs; istanojevic@gmail.com

activation followed by sustained astrogliosis, the response of resident microglial to hippocampal neuronal loss that progressively worsens over 3 weeks (Dragic et al., 2019b, 2021; Haga et al., 2002; Little et al., 2002, 2012), as well as a cognitive deficit in various tasks similar to human neurodegenerative disorders such as Alzheimer's disease and temporal lobe epilepsy (Chvojkova et al., 2021; Corvino et al., 2013; Geloso et al., 2011; Lattanzi et al., 2013; Lee et al., 2016; Pompili et al., 2020; Trabucco et al., 2009; Ye et al., 2020). Thus, TMT neurotoxicity is a valuable tool for studying changes in molecular signatures of glial cells during the progression of neurodegeneration that accompanies hippocampal dysfunction.

In general, glial cells, microglia, and astrocytes are crucial in monitoring, maintaining, and preserving the metabolic and structural integrity of the central nervous system (CNS), and respond to noxious stimuli and insults to the brain. Alterations in CNS homeostasis immediately lead to changes in microglial cells morphology and functional polarization toward one of the two complex phenotypes, detrimental that release proinflammatory cytokines and reactive oxygen species (ROS) and reactive nitrogen species or prorepair, an antiinflammatory phenotype that express molecular markers such as arginase-1 (Arg1) (Illes et al., 2020; Zabel & Kirsch, 2013), with a full repertoire of transitional states between them. In response to brain injury, astrocytes assume reactive states that may be discriminated based on the proliferation and induction of proinflammatory mediators and ROS (Verkhratsky et al., 2014). Furthermore, different polarized states of reactive astrocytes are characterized, determined as dominantly harmful, a proinflammatory type that might releases the neurotoxic complement C3 directly leading to neuron death, and the dominantly neuroprotective type (Liddelow & Barres, 2017), but also with the repertoire of transitional microenvironment-dependent states.

Communication between astrocytes, microglia, and degenerating neurons is mediated via different signaling molecules, and one of the strongest is adenosine triphosphate (ATP) (Sperlagh & Illes, 2007). A large amount of extracellular ATP, released from injured neurons and activated glial cells, acts as a "danger signal" and activates specific ligand-gated P2X channels and G-protein-coupled P2Y receptors (Burnstock, 2017; Di Virgilio et al., 2009; Sperlagh & Illes, 2007), promoting microglial chemotaxis and phagocytosis as well as the release of proinflammatory cytokines (Bernier et al., 2013; Franke et al., 2012; Haynes et al., 2006; Illes et al., 2020). Enzymes responsible for calibrating the duration, and degree of P2 receptor activation are functionally coupled membrane-bound ectonucleotidases named ecto-nucleoside triphosphate diphosphohydrolase 1 (NTPDase1/CD39) and ecto-5′ nucleotidase (eN/CD73) that rapidly hydrolyze ATP to adenosine (Grkovic et al., 2019a; Matyash et al., 2017; Zimmermann et al., 2012). NTPDase1/CD39 is dominantly expressed at microglia and endothelial cells and hydrolyzes ATP and adenosine diphosphate (ADP) to adenosine monophosphate (AMP) (Braun et al., 2000; Grkovic et al., 2019b; Matyash et al., 2017; Robson et al., 2006; Zimmermann et al., 2012). The resulting AMP is hydrolyzed to adenosine by eN/CD73, widely expressed in the hippocampus (Grkovic et al., 2019a, 2019b; Zimmermann et al., 2012). Adenosine G-protein-coupled receptors (A_1R, $A_{2A}R$, $A_{2B}R$, and A_3R) mediate modulatory effects of adenosine in an inflammatory environment (Hasko & Cronstein, 2013; Nedeljkovic, 2019). The two ectonucleotidases act together as an immune checkpoint since they determine the ATP/adenosine ratio and the inflammatory status of the tissue. Therefore, an altered function of NTPDase1/CD39 and eN/CD73 and dysregulation of the purinergic signaling are largely implicated in the pathophysiology of several neurological diseases, including Alzheimer's and Parkinson disease, multiple sclerosis, and astroglioma (Burnstock, 2017), but their cell-specific localization during neurodegeneration is rarely explored. Furthermore, NTPDase1/CD39 and eN/CD73 represent promising pharmacological targets in the treatment of neuroinflammatory processes (Antonioli et al., 2013).

It has been previously described an early change in astrocyte morphology that precedes neuronal loss, particular reactive astrocyte phenotypes, and their dynamic remodeling after TMT intoxication (Dragic et al., 2019b). It was also found that TMT-induced mitochondrial depolarization is independent of extracellular Ca^{2+} and disturbed antioxidative defense, but also upregulated main proinflammatory factors and components of signaling pathways responsible for astrocyte reactivity, and markers of proinflammatory subtype of astrocytes in vitro (Dragic et al., 2021). Induction of $P2X_2R$ in glial cells has been reported after TMT intoxication (Latini et al., 2010), but the involvement of other purinergic signaling components has not been explored. The main goal of the present study was to explore the cell-specific localization of NTPDase1/CD39 and eN/CD73 and the expression of purinergic receptors specific for microglia in the early and the late stage of hippocampal neurodegeneration induced by TMT. Furthermore, there is no information on whether TMT-induced inflammation in rats is caused by reactive microglia and/or astrocytes. Thus, in the present study, we analyzed NTPDase1/CD39 and eN/CD73, and purinergic receptors expression patterns in the context of activation of glial cells, inflammation, and its potential resolution after TMT intoxication. We also hypothesized that components of purinergic signaling may assign functional states of glial cells.

Material and Methods

Animals, Surgical Procedure, and Treatment

Two-month-old female rats of the Wistar strain (200–220 g) maintained in the local animal facility were used in the study. Appropriate actions were taken to alleviate the pain and discomfort of the animals following the compliance with the European Communities Council Directive (2010/

63/EU) for animal experiments, and the research procedures were approved by the Ethical Committee for the Use of Laboratory Animals. Animals were housed 3–4/cage, in a 12 h light/dark regime, constant humidity and temperature, and free access to food and water.

It was previously shown that TMT-induced hippocampal neurodegeneration and gliosis, the pattern of which was comparable in adult rats of both sexes (Corvino et al., 2015; Dragic et al., 2019b; Geloso et al., 2011; Haga et al., 2002; Little et al., 2012; Trabucco et al., 2009). However, given that the expression of ectonucleotidases in the brain is modulated/regulated by gonadal steroids and differs in two sexes (Grkovic et al., 2019b; Mitrovic et al., 2016, 2017), the study was performed in female rats, bilaterally ovariectomized 3 weeks before TMT injection as we described previously (Dragic et al., 2019b).

On day zero, animals of the TMT group received TMT (8 mg/kg dissolved in 1 mL 0.9% w/v saline) (in the form of a single intraperitoneal [i.p.] injection), whereas the control (Ctrl) group received an adequate volume of 0.9% saline solution. The animals were returned to their cages, and monitored for unusual signs of behavior until sacrifice, as reported previously (Dragic et al., 2019b). At 7 and 21 days post intoxication (dpi), animals of TMT and age-matched Ctrl groups (10 animals/group) were sacrificed by decapitation (Harvard apparatus, Holliston, MA, USA).

Histochemistry, Immunohistochemistry, and Immunofluorescence Microscopy

Brains ($n = 5$ per group) were carefully removed from the skull, fixed in 4% paraformaldehyde for 24 h, cryoprotected in graded sucrose (10%–30% in 0.2 M phosphate buffer), and stored at 4 °C, as described before (Dragic et al., 2019b; Grkovic et al., 2019b). The brains were cryosectioned in serial 25 μm thick coronal sections and the sections at 3.12–3.84 mm anteroposterior to Bregma were air-dried and stored at – 20 °C until use.

Nissl Staining. Alterations in hippocampal cytoarchitecture induced by TMT injection were evaluated by Nissl staining. Sections were kept in 0.5% thionine solution for 20 min, washed in tap water, dehydrated in graded ethanol (70%–100%), cleared in xylene for 2×5 min, and covered with DPX-mounting medium (Sigma Aldrich, USA).

Immunohistochemistry and Immunofluorescence. Slides were kept at room temperature (RT) for 30 min before staining. After washing in phosphate-buffered saline (PBS), slides were put in 0.3% H_2O_2 in methanol for 20 min, to block endogenous peroxidase, and then immersed in 5% donkey normal serum at RT for 1 h to block nonspecific binding. Sections were probed with primary antibodies, overnight at 4 °C in a humid chamber. After washing in PBS (3×5 min), sections were incubated with horseradish peroxidase (HRP)-conjugated secondary antibodies (2 h, RT in a humid chamber). The list of antibodies used for immunohistochemistry (IHC) and immunofluorescence (IF) is presented in Table 1. The immunoreaction was visualized with 3,3′S-diaminobenzidine-tetrahydrochloride (Abcam, UK), which is converted to the insoluble brown precipitate by HRP. Sections were washed in distilled water, dehydrated in graded ethanol solutions (70%–100%), cleared in xylene, and mounted with the use of DPX-mounting medium (Sigma Aldrich, USA). Sections were analyzed under a LEITZ DM RB light microscope (Leica Mikroskopie & Systems GmbH, Wetzlar, Germany), equipped with a LEICA DFC320 CCD camera (Leica Microsystems Ltd, Heerbrugg, Switzerland), and LEICA DFC Twain Software (Leica, Germany). All images were captured at 40× magnification.

The identical protocol has been applied for double and triple IF staining, with the omission of the methanol/H_2O_2 step. After incubation with primary antibodies (Table 1), sections were probed with fluorescence dye-labeled secondary antibodies and mounted with Mowiol (Calbiochem, La Jolla, CA). For double and triple IF staining, primary and secondary antibodies were separately applied for each labeling. Sections incubated without primary antibodies or with rat preimmune sera were used as negative Ctrls. Sections were analyzed by a confocal laser-scanning microscope (LSM 510, Carl Zeiss GmbH, Jena, Germany), using Ar multiline (457, 478, 488, and 514 nm), HeNe (543 nm), and HeNe (643 nm) lasers using 63× (2× digital zoom) DIC oil, 40× and monochrome camera AxioCam ICm1 camera (Carl Zeiss GmbH, Germany).

Enzyme Histochemistry. Ectonucleotidase enzyme histochemistry based on the ATP/ADP- and AMP-hydrolyzing activities of NTPDase1/CD39 and eN/CD73, respectively, have been applied (Dragic et al., 2019a; Grkovic et al., 2019b). Briefly, cryosections were preincubated for 30 min at RT in Tris-maleate sucrose (TMS) buffer, containing 0.25 M sucrose, 50 mM Tris-maleate, 2 mM $MgCl_2$ (pH 7.4), and 2 mM levamisole, to inhibit tissue nonspecific alkaline phosphatase. The enzyme reaction was carried out at 37 °C/60 min, in TMS buffer, containing 2 mM $Pb(NO3)_2$, 5 mM $MnCl_2$, 3% dextran T250, and 1 mM substrate (ATP, ADP, or AMP). After thorough washing, slides were immersed in 1% (v/v) $(NH_4)_2S$, and the product of enzyme reaction was visualized as an insoluble brown precipitate at a site of the enzyme activity. After dehydration in graded ethanol solutions (70%–100% EtOH, and 100% xylol), slides were mounted with a DPX-mounting medium (Sigma Aldrich, USA). The sections were examined under a LEITZ DM RB light microscope (Leica Mikroskopie & Systems GmbH, Wetzlar, Germany), equipped with a LEICA DFC320 CCD camera (Leica Microsystems Ltd, Heerbrugg, Switzerland)

Table 1. List of Antibodies.

Antibody	Source and type	Used dilution	Manufacturer
Iba1	Goat, polyclonal	1:400$^{IHC, IF}$	Abcam ab5076, RRID: AB_2224402
CD73, rNu-9L(I4,I5)	Rabbit, polyclonal	1:300$^{IHC, IF}$	Ectonucleotidases-ab.com
CD39, mN1-2C(I4,I5)	Guinea pig, polyclonal	1:200^{IF}	Ectonucleotidases-ab.com
Arg1	Rabbit, polyclonal	1:200^{IF}	Sigma AV45673, RRID: AB_1844986
iNOS	Rabbit, polyclonal	1:200^{IF}	Abcam ab15323, RRID: AB_301857
CD68	Rabbit, polyclonal	1:200^{IF}	Abcam ab125212, RRID: AB_10975465
$P2Y_{12}$	Rabbit, polyclonal	1:300^{IF}	Sigma P4817, RRID: AB_261954
GFAP	Mouse, monoclonal	1:100^{IF}	UC Davis/NIH NeuroMab Facility (73–240), RRID: AB_10672298
GFAP	Rabbit, polyclonal	1:500^{IF}	DAKO, Agilent Z0334, RRID: AB_10013382
C3	Goat, polyclonal	1:300^{IF}	Thermo Fisher Scientific PA1-29715 RRID: AB_AB_2066730
TNF-α	Goat, polyclonal	1:100^{IF}	Santa Cruz Biotechnology, sc-1350, RRID: AB_2204365
IL-10	Goat, polyclonal	1:100^{IF}	Santa Cruz Biotechnology, sc-1783, RRID: AB_2125115
NF-kB	Rabbit, polyclonal	1:100^{IF}	Santa Cruz Biotechnology, sc-109, RRID: AB_632039
IL-1β/IL-1F2	Goat, polyclonal	1:100^{IF}	R&D Systems, AF-501-NA, RRID: AB_ 354508
$P2Y_1$	Rabbit, polyclonal	1:300^{IF}	Alomone Labs; APR-0009, RRID: AB_2040070
A_{2A}	Rabbit, polyclonal	1:300 ^{IF}	Abcam, ab3461, RRID: AB_303823
$P2X_7$	Rabbit, polyclonal	1:400 ^{IF}	Alomone Labs, APR-004, RRID: AB_2040068
A_1R	Rabbit, polyclonal	1:200 ^{IF}	Novus Biologicals, NB300-549, RRID: AB_10002337
Anti-mouse IgG Alexa Fluor 488	Donkey, polyclonal	1:400^{IF}	Invitrogen A21202, RRID: AB_141607
Anti-goat IgG Alexa Fluor 488	Donkey, polyclonal	1:400^{IF}	Invitrogen A-11055, RRID: AB_142672
Anti-rabbit IgG Alexa Fluor 555	Donkey, polyclonal	1:400^{IF}	Invitrogen A-21428, RRID: AB_141784
Anti-mouse IgG Alexa Fluor 647	Donkey, polyclonal	1:400^{IF}	Thermo Fisher Scientific A-31571, RRID: AB_162542
Anti-goat HRP-conjugated IgG	Rabbit, polyclonal	1:200^{IHC}	R&D Systems, HAF017 RRID: AB_56258
Anti-rabbit IgG Alexa Fluor 488	Donkey, polyclonal	1:400^{IF}	Invitrogen A-21206, RRID: AB_141708
Anti-guinea pig IgG Alexa Fluor 555	Goat, polyclonal	1:200^{IF}	Invitrogen A-21435, RRID: AB_2535856
Anti-mouse HRP-conjugated IgG	Goat, polyclonal	1:200^{IHC}	R&D Systems, HAF007 RRID: AB_562588
Anti-goat HRP-conjugated IgG	Rabbit, polyclonal	1:200^{IHC}	R&D Systems, HAF017 RRID: AB_56258

Note. Arg1 = arginase-1; GFAP = glial fibrillary acidic protein; HRP = horseradish peroxide; IF = immunofluorescence; IgG = immunoglobulin G; IHC = immunohistochemistry; IL-10 = interleukin-10; IL-1F2 = interleukin-1F2; IL-1β = interleukin-1β; iNOS = inducible nitric oxide synthase; NF-kB = nuclear factor-kB; TNF-α = tumor necrosis factor-α.

and analyzed using LEICA DFC Twain Software (Leica, Germany).

IF Quantification. Raw multiimage IF micrographs were used to measure integrated fluorescence density expressed as arbitrary units (AUs) and the density confined within five predefined regions of interest (ROIs), with background fluorescence subtraction for at least three images per ROI and $n = 5$ sections per animal per group (JACoP ImageJ plugin). A degree of overlap and correlation between multiple channels was estimated by calculating Pearson's correlation coefficient (PCC) (Dunn et al., 2011). PCC is a statistical parameter that reflects both cooccurrence (degree at which intensities of two channels for each pixel are beyond or above the threshold), and correlation (pixel-for-pixel proportionality in the signal levels of the two channels). PCC values range from 1 (for two images whose fluorescence intensities are perfectly, linearly related) to -1 (for two images whose fluorescence intensities are perfectly, but inversely, related to one another). Values near zero reflect distributions of probes that are uncorrelated with one another. The results are expressed as mean PCC ± standard error of the mean (SEM).

Gene Expression Analysis by Quantitative Reverse Transcriptase-Polymerase Chain Reaction

Total RNA was extracted from the hippocampal formation (7 and 21 dpi and appropriate age-matched Ctrls, $n = 5$ animals per group) using TRIzol Reagent (Invitrogen, Carlsbad, CA, USA), according to the manufacturer's instructions. Purity and the concentration of isolated RNA were assessed by OD_{260}/OD_{280} and OD_{260}, respectively. Complementary DNA (cDNA) was synthesized using a High-Capacity cDNA Reverse Transcription Kit (ThermoFisher Scientific, MA, USA) and stored at –20 °C

Table 2. Primer Sequences Used for RT-qPCR.

Gene	Sequence (5′- −3′)	Length (bp)
NTPDase1 (*Entpd1*)	TCAAGGACCCGTGCTTTTAC TCTGGTGGCACTGTTCGTAG	150
eN (*Nt5e*)	CAAATCTGCCTCTGGAAAGC ACCTTCCAGAAGGACCCTGT	160
$P2X_4R$ (*P2rx4*)	ACCAGGAAACGGACTCTGTG TCACGGTGACGATCATGTTGG	168
$P2X_7R$ (*P2rx7*)	ATTGTTAGGCCAATGGCAAG AACACCTTCACCGTCTCCAC	190
$P2Y_2R$ (*P2ry2*)	TCACCCGCACCCTCTATTAC GCCAGGAAGTAGAGCACAGG	139
$P2Y_6R$ (*P2ry6*)	CAGTTATGGAGCGGGACAAT GTAAACTGGGGGTAGCAGCA	104
$P2Y_{12}R$ (*P2ry12*)	CGAAACCAAGTCACTGAGAGGA CCAGGAATGGAGGTGGTGTTG	162
$P2Y_1R$ *(P2ry1)*	CTGGATCTTCGGGGATGTTA CTGCCCAGAGACTTGAGAGG	138
A_1R (*Adora1*)	GTGATTTGGGCTGTGAAGGT GAGCTCTGGGTGAGGATGAG	194
$A_{2A}R$ (*Adora2a*)	TGCAGAACGTCACCAACTTC CAAAACAGGCGAAGAAGAGG	141
$A_{2B}R$ (*Adora2b*)	CGTCCCGCTCAGGTATAAAG CCAGGAAAGGAGTCAGTCCA	104
A_3R (*Adora3*)	TTCTTGTTTGCCTTGTGCTG AGGGTTCATCATGGAGTTCG	129
IL-1β (*Il1b*)	CACCTCTCAAGCAGAGCACAG GGGTTCCATGGTGAAGTCAAC	79
TNFα (*Tnf*)	CCCCCATTACTCTGACCCCT CCCAGAGCCACAATTCCCTT	88
IL-6 (*Il6*)	CCGGAGAGGAGACTTCACAG ACAGTGCATCATCGCTGTTC	160
IL-10 (*Il10*)	GCTCAGCACTGCTATGTTGC GTCTGGCTGACTGGGAAGTG	106
C3 (*C3*)	GCGGTACTACCAGACCATCG CTTCTGGCACGACCTTCAGT	166
iNOS (*Nos2*)	ACACAGTGTCGCTGGTTTGA AACTCTGCTGTTCTCCGTGG	125
Arg1 (*Arg1*)	CTGTGGTAGCAGAGACCCAGA GGTTGTCAGCGGAGTGTTGA	161
S100a10 (*S100a10*)	GTACCCACACCTTGATGCGT CGAAAGCTCCTCTGTCATTGG	130
CycA (*Ppia*)	CAAAGTTCCAAAGACAGCAGAAAA CCACCCTGGCACATGAAT	114
HPRT1 (*Hprt1*)	GGTCCATTCCTATGACTGTAGATTTT CAATCAAGACGTTCTTTCCAGTT	126
GAPDH (*Gapdh*)	CAACTCCCTCAAGATTGTCAGCAA GGCATGGACTGTGGTCATGA	118

Note. Arg1 = arginase-1; CycA = cyclophilin A; GAPDH = glyceraldehyde-3-phosphate dehydrogenase; HPRT1 = hypoxanthine phosphoribosyltransferase 1; IL-10 = interleukin-10; IL-1β = interleukin-1β; IL-6 = interleukin-6; iNOS = inducible nitric oxide synthase; RT-qPCR=quantitative reverse transcriptase-polymerase chain reaction; TNF-α = tumor necrosis factor-α.

until use. Quantitative real-time polymerase chain reaction (PCR) was performed using Power SYBR™ Green PCR Master Mix (Applied Biosystems, MA, USA) and ABI Prism 7000 Sequence Detection System (Applied Biosystems, MA, USA) under the following conditions: 10 min of enzyme activation at 95 °C, 40 cycles of 15 s denaturation at 95 °C, 30 s annealing at 60 °C, 30 s amplification at 72 °C, and 5 s fluorescence measurement at 72 °C. Primer sequences used for the amplification are given in Table 2. To compare the relative expression levels of the studied transcripts, we validated three *housekeeping genes*: glyceraldehyde-3-phosphate dehydrogenase (*Gapdh*), cyclophilin A (*CycA*), and hypoxanthine-

guanine phosphoribosyltransferase (*Hprt*). Cycle threshold (Ct) values in all examined animals for all *housekeeping genes* were within the same half of the same cycle making it all acceptable as a reference gene. The expression profiles of genes that we studied were comparable when normalized to *all housekeeping genes*. Thus, for relative quantification of target genes, we used the $2^{-\Delta\Delta Ct}$ method, using *CycA* as a reference gene. Samples obtained from five animals for each experimental group were run in duplicate. Amplification efficacy was assessed by the generation of internal standard curves by several-fold dilutions of generated cDNA while melting curve analysis at the end of each experiment was used to confirm the formation of a single PCR product. The results were expressed as the abundance of target messenger RNA (mRNA)/CycA-mRNA at 7 and 21 dpi relative to a corresponding Ctrl ± standard deviation (SD). Relative expressions of target genes normalized against CycA used as a housekeeping gene are shown in Supplementary Table 1.

Statistical Analysis

Data were analyzed for normality and appropriate parametric tests were used. All values are presented as mean ± SD or SEM. Between-group comparisons for 7 and 21 dpi were analyzed using an unpaired *t*-test. The values of $p < .05$ or less were considered statistically significant. For all statistical analyses, Graphpad Prism 5.04 (Graphpad) software was used.

Results

Spatiotemporal Patterns of Neurodegeneration and Gliosis After TMT Exposure

TMT-induced hippocampal degeneration was confirmed by Nissl staining (Figure 1a). As we have shown previously (Dragic et al., 2019b), cell injury was observed in the hilar/proximal CA3 (hilus/pCA3) at 7 dpi. This is followed by the almost complete disappearance of staining in neuronal somata in CA1 and the proximal and medial CA3 (p/mCA3) regions at 21 dpi (Figure 1a), as already reported (Geloso et al., 2011; Haga et al., 2002; Latini et al., 2010; Little et al., 2012). As reported previously (Dragic et al., 2019b), immunostaining of astrocyte marker glial fibrillary acidic protein (GFAP) showed the presence of pronounced astrogliosis at 7 dpi as well as 21 dpi (Figure 1b).

A great morphological diversity of reactive microglia was observed (Figure 1c and d). Specifically, highly ramified Iba1-immunoreactive (*ir*) cells, evenly distributed in the Ctrl hippocampal tissue (Figure 1c), were gradually transformed to rod Iba1-*ir* cells in synaptic layers of CA1 and the hilar/pCA3 at 4 dpi (data not shown). Besides rod shape, a range of other reactive Iba1-*ir* morphotypes was observed, from hyperramified to bushy/amoeboid. At 7 dpi, rod Iba1-*ir* cells populated the synaptic layers in the entire CA1 and the hilar/pCA3 sectors, while $Iba1^+$cells in the neuronal cell layers attained amoeboid morphology (Figure 1c and d). At 21 dpi, most of the heavily labeled $Iba1^+$ cells with pronounced amoeboid morphology were located in the pyramidal cell layer and especially in p/mCA3 region. Interestingly, rod Iba1-*ir* cells were not observed in the hilar/pCA3, whereas the hilar area and granular cell layer appeared completely without Iba1-*ir* at the latest time point (Figure 1c).

Expression of NTPDase1/CD39, eN/CD73, and Purinoreceptors Involved in Microglial Reactivity

The main goal of the present study was to explore the involvement of the purinergic signaling system in TMT-induced hippocampal neurodegeneration and gliosis. We first analyzed the expression of genes encoding NTPDase1/CD39 and eN/CD73. There was a significant increase in the relative expression of NTPDase1/CD39-mRNA in the hippocampal tissue at 7 and 21 dpi ($p < .01$ and $p < .0001$, respectively) when compared with age-match Ctrls. Although the relative expression of eN/CD73-mRNA in the hippocampal tissue at 7 dpi did not change, the enzyme mRNA levels significantly increased at 21 dpi when compared with age-match Ctrl ($p < .01$) (Figure 2a).

The pattern of the enzyme activity in the hippocampus and the localization of upregulated NTPDase1/CD39 in response to TMT were determined by enzyme histochemistry using ATP and ADP as a substrate (Braun et al., 2000; Grkovic et al., 2019b). In accordance with well-known data (Braun et al., 2000; Grkovic et al., 2019b; Robson et al., 2006), the typical patterns of histochemical reaction for ATPase/ADPase activities were observed in Ctrl hippocampi, labeling synaptic layers, ramified microglia, and endothelial cells typical for NTPDase1/CD39 (Figure 2b). In the first four days after intoxication (data not shown), reduction of staining in neuropil through hippocampus was noticed particularly when ADP was used as a substrate. This reduction was accompanied by a parallel increase of lead-phosphate deposition that nicely delineated cellular membranes of microglia. At 7 dpi lead-phosphate depositions delineated reactive microglia that covered the strata but also entered the neuronal layers (Figure 2b). At 21 dpi, activated microglia accounted for most of the enhanced ATPase/ADPase activities, revealing strong staining of CA strata, while dentate gyrus (DG) was mostly without reaction (Figure 2b). The obtained patterns of ATP/ADP enzyme activities closely corresponded to Iba1-*ir* (Figure 1c), suggesting that reactive microglial cells upregulated NTPDase1/CD39 after the exposure to TMT.

eN/CD73 activity and localization in response to TMT were determined using AMP-based enzyme histochemistry (Figure 2c) and eN/CD73-directed immunocytochemistry (Figure 2d). In intact hippocampal tissue, diffuse histochemical reaction and eN/CD73-*ir* were observed in synaptic layers,

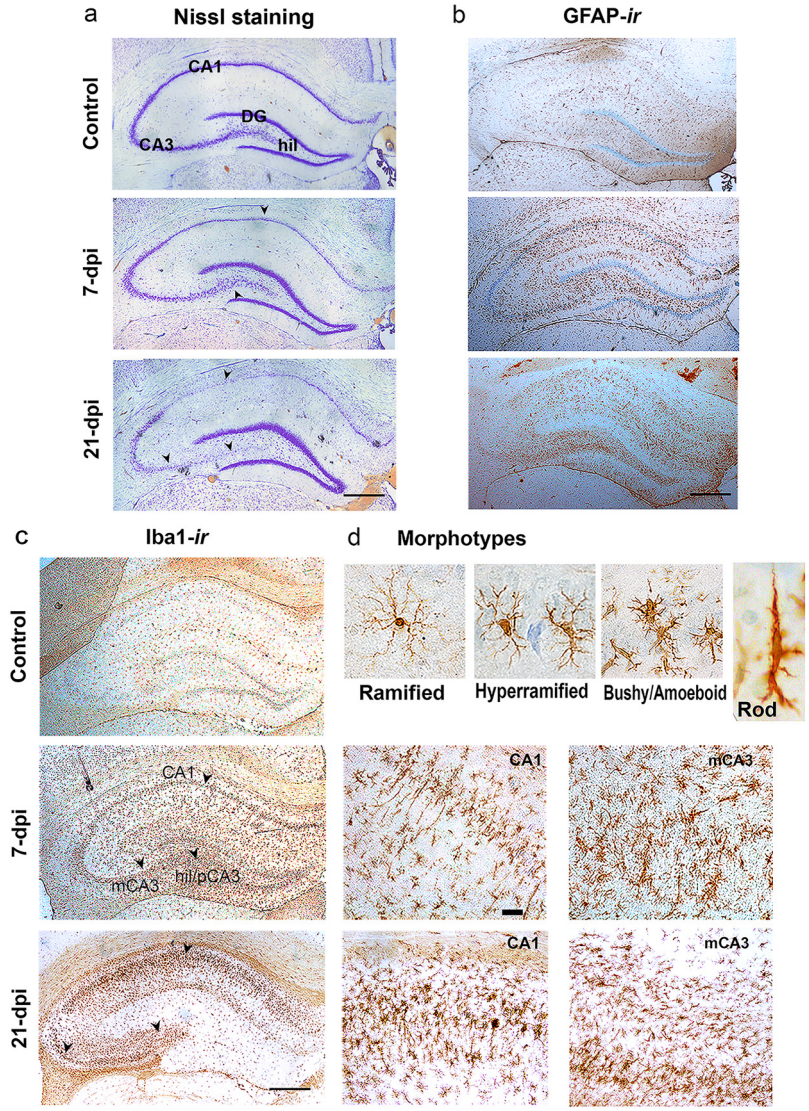

Figure 1. Spatiotemporal pattern of hippocampal neurodegeneration and gliosis after TMT exposure (a) thionine staining of coronal sections obtained from control animals and at 7 and 21 dpi. Arrowheads indicated injured neuronal cell layers in the hippocampus. Scale bar = 500 μm. (b) Immunohistochemical staining of GFAP in control animals and at 7 and 21 dpi. Scale bar = 500 μm. (c) Immunohistochemical staining of Iba1 in the whole hippocampal area and corresponding enlarged CA1 and mCA3 at 7 and 21 dpi. Scale bar = 500 μm (under 5× magnification), and 100 μm (under 20× magnification). (d) Representative images of different Iba1-*ir* morphological phenotypes are observed in control and after TMT exposure.

Note. dpi = days post intoxication; GFAP = glial fibrillary acidic protein; *ir* = immunoreactive; mCA3 = medial CA3; TMT = trimethyltin.

while neuronal cell layers remained unstained, as were shown previously (Dragic et al., 2019a; Grkovic et al., 2019b). From 7 dpi and afterward, products of AMPase activity were accumulated in the neuronal strata, infiltrating within neuronal cell layers (Figure 2c). eN/CD73-*ir* completely reflected patterns observed by AMPase, depicted individual round-shaped elements that covered neuronal layers and were most noticeable at the late stage of TMT-induced neurodegeneration (21 dpi, Figure 2d). Cellular localization of eN/CD73-*ir* was determined by triple IF directed to GFAP, Iba1, and eN/CD73 (Figure 3a). At 7 and 21 dpi, eN/CD73-*ir* overlapped with Iba1-*ir* at amoeboid cells infiltrated within neuronal cell layers, while colocalization with GFAP-*ir* was not observed. The colocalization of main microglial ectonucleotidase NTPDase1/CD39, and eN/CD73 was demonstrated by double-IF labeling, which showed colocalization of NTPDase1/CD39 and eN/CD73 at amoeboid cells, while ramified and rod NTPDase1/CD39-*ir* cells within synaptic layers did not show eN/CD73-*ir* (Figure 3b). The degree of colocalization was estimated by the Pearson correlation coefficient (PCC) (Figure 3c). The raising PCC values indicated increase in colocalization of Iba1/eN/CD73 ($p < .0001$) and

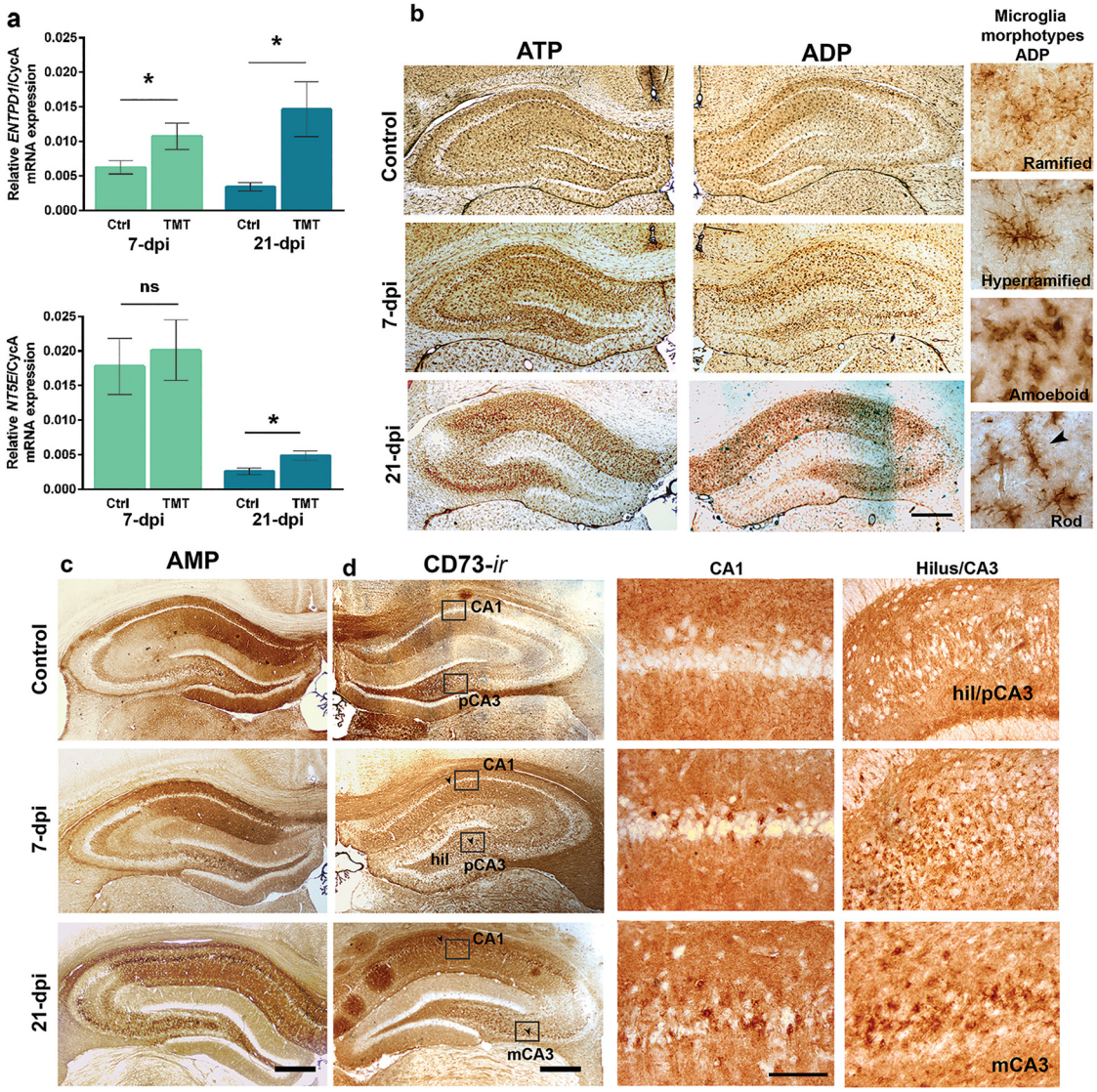

Figure 2. Expression and activity of NTPDase1/CD39 and eN/CD73 in the hippocampal region after TMT exposure (a) RT-qPCR analysis of genes encoding NTPDase1/CD39 and eN/CD73 in the Ctrl hippocampal tissue, 7 and 21 dpi, respectively. Bars represent mean mRNA expression of target gene relative to CycA ± SD. Significance shown inside the graphs: *$p < .05$ or less compared to age-match Ctrl. In the presence of ATP or ADP (b) and AMP (c) as substrate, enzyme histochemistry labeled cells and structures correspond to ectonucleotidase activities in the hippocampal region of Ctrl, 7 and 21 dpi. Microglial cells were clearly labeled by ATP and ADP enzyme histochemistry. High magnifications of microglial morphotypes observed by ADPase enzyme histochemistry were inserted. (d) eN/CD73-*ir* in the hippocampal region of Ctrl section, 7 and 21 dpi. Rectangles show eN/CD73-*ir* areas—CA1, hil/pCA3 and mCA3 captured under higher magnification. eN/CD73 depicted individual round-shaped elements in the neuronal layers and were most noticeable at 21 dpi. Scale bar = 500 μm (under 5× magnification), and 50 μm (under 40× magnification).

Note. ADP = adenosine diphosphate; AMP = adenosine monophosphate; ATP = adenosine triphosphate; Ctrl = control; CycA = cyclophilin A; dpi = days post intoxication; eN/CD73 = ecto-5′ nucleotidase; hil/pCA3 = hilar/proximal CA3; *ir* = immunoreactive; mCA3 = medial CA3; mRNA = messenger RNA; NTPDase1/CD39 = ectonucleoside triphosphate diphosphohydrolase 1; RT-qPCR = quantitative reverse transcriptase-polymerase chain reaction; SD = standard deviation; TMT = trimethyltin.

NTPDase1/CD39-eN/CD73 ($p < .0001$) signals at both time points after TMT exposure, whereas negative PCC values for GFAP-*ir* and eN/CD73-*ir* ($p = .32$) corroborated the lack of astrocytic expression of eN/CD73 after TMT. The results pointed to the marked induction of NTPDase1/CD39 by $Iba1^+$ cells, and the colocalization with eN/CD73 at amoeboid $Iba1^+$ cells after TMT exposure (Figure 3c).

Since the role of extracellular ATP is closely related to its breakdown products, changes in mRNA expression of ATP/ADP-sensitive P2 and adenosine P1 receptors in the

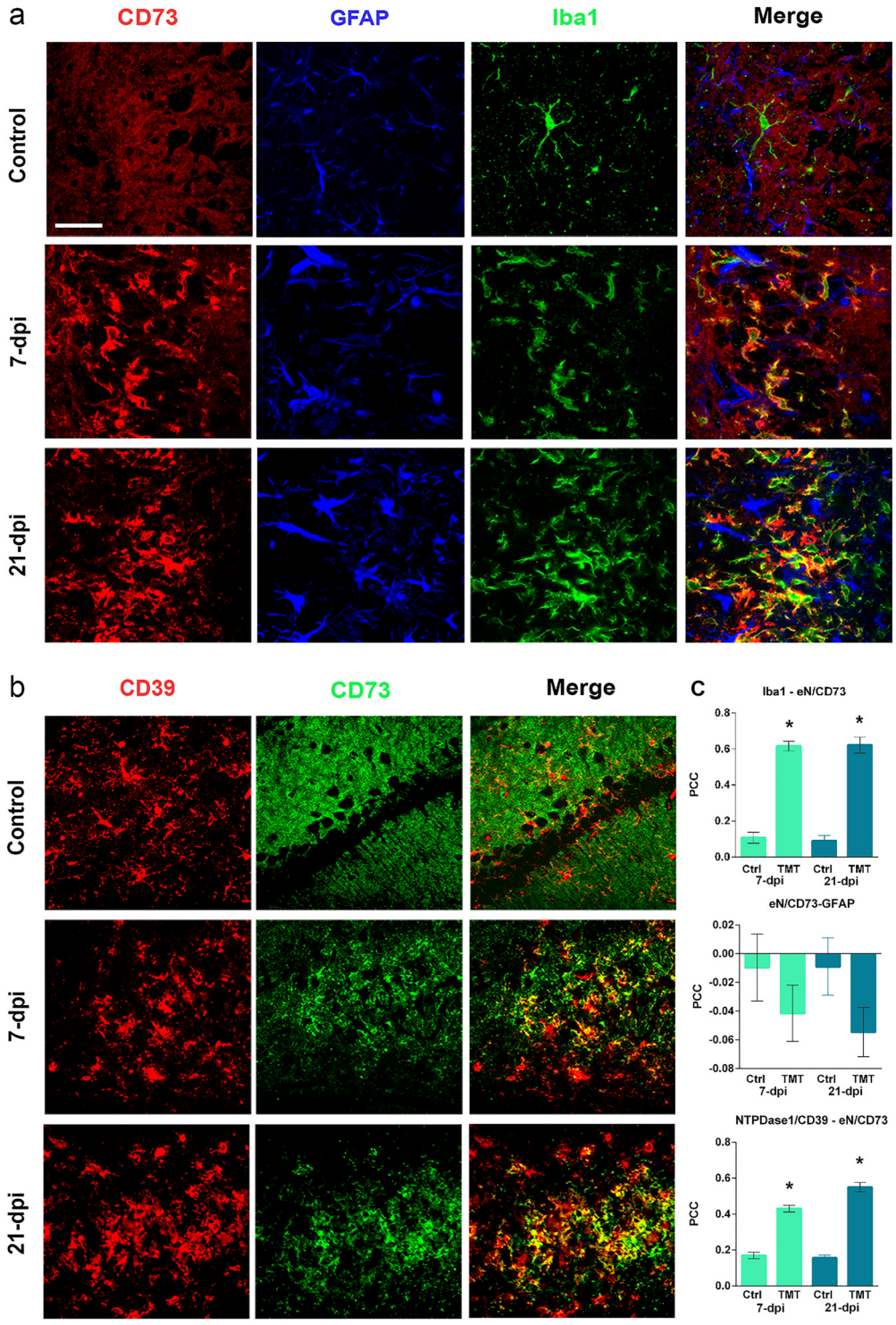

Figure 3. Identification of cells that upregulate eN/CD73 in the hippocampal region after TMT exposure (a) triple IF labeling directed to eN/CD73 (red), astrocyte marker GFAP (blue), and microglial marker Iba1 (green) in the Ctrl, 7 and 21 dpi hippocampi. Overlaid images (merge) reveal the overlapping signal corresponding to Iba1-*ir* and eN/CD73-*ir* at 7 and 21 dpi. (b) Double-IF labeling directed to NTPDase1/CD39 (red) and eN/CD73 (green), showing the overlapping signals (merge) at 7 and 21 dpi. Scale bar = 50 μm. (c) PCC indicates the level of signal overlap between Iba1-*ir* and eN/CD73-*ir*, eN/CD73-*ir* and GFAP-*ir* and NTPDase1/CD39-*ir* and eN/CD73-*ir*. Bars show mean PCC ± SEM, from 3 ROI selected from 5 sections. Significance shown inside the graphs: *$p < .05$ or less compared to age-match Ctrl.
Note. Ctrl = control; dpi = days post intoxication; eN/CD73 = ecto-5′ nucleotidase; *ir* = immunoreactive; NTPDase1/CD39 = ecto-nucleoside triphosphate diphosphohydrolase 1; GFAP = glial fibrillary acidic protein; IF = immunofluorescence; PCC = Pearson correlation coefficient; SEM = standard error of the mean; ROI = region of interest; TMT = trimethyltin.

hippocampus during TMT-induced neurodegeneration were explored (Figure 4). Regarding ATP/ADP-sensitive P2 receptors mainly expressed by microglia (Illes et al., 2020), a significant increase in the relative abundance of $P2X_4R$-, $P2Y_2R$-, and $P2Y_6R$-mRNA levels were observed, at both 7 dpi ($p < .0001$, $p < .0001$, $p < .0001$, respectively) and 21 dpi ($p < .001$, $p < 0.0001$, $p < .001$, respectively) when compared to age-matched Ctrls (Figure 4). The $P2Y_{12}R$-mRNA level of the specific microglial receptor (Illes et al., 2020) was robustly increased at 7 dpi ($p < .0001$) while a slight increase was observed at 21 dpi ($p < .05$) (Figure 4). $P2X_7R$- and $P2Y_1R$-mRNA levels were significantly increased at both 7- ($p < .001$ and $p < .05$, respectively) and 21 dpi ($p < .01$ and $p < .001$, respectively), when compared to age-match Ctrl. Furthermore, analysis of adenosine P1 receptors showed an increase in A_3R-mRNA levels at both 7 and 21 dpi when compared to age-match Ctrl ($p < .001$ and $p < .01$, respectively), together with induction of A_1R-mRNA relative abundances at 21 dpi ($p < .01$, Figure 4). There are no changes in $A_{2B}R$-mRNA relative abundances at both 7 and 21 dpi. Relative expressions of target genes for all tested time points are shown in Supplemental Table 1.

The Inflammatory Status of the Hippocampal Tissue After TMT Exposure

It is known that activated glial cells develop functional phenotypes, which may be roughly categorized as proinflammatory or antiinflammatory. Therefore, we first assessed the inflammatory status of the hippocampal tissue at the early (7 dpi) and the late (21 dpi) stage of TMT-induced neurodegeneration by determining the expression of several inflammatory markers. As shown in Figure 5, only tumor necrosis factor-α (TNF-α)-mRNA level was significantly increased at 7 dpi when compared to Ctrl ($p < 0.0001$), while interleukin (IL)-1β-, IL-6-, IL-10-mRNA relative abundances were significantly increased at 21 dpi ($p < .01$, $p < .01$, and $p < .001$, respectively, Figure 5). We also examined the main markers of two extreme polarization states of microglia/macrophages (inducible nitric oxide synthase [iNOS] and Arg1), as well as C3 and S100a10 as markers that are often used to discriminate between functional states of astrocytes. iNOS-, C3- and S100a10-mRNA levels were significantly increased at both 7- ($p < .001$, $p < .0001$, $p < .001$, respectively) and 21 dpi ($p < .01$, $p < .0001$, $p < .05$, respectively) when compared to age-match Ctrl (Figure 5). Arg1-mRNA level was decreased at 7 dpi ($p < .0001$), while no changes were detected at 21 dpi when compared to age-match Ctrl (Figure 5). Relative expressions of target genes for all tested time points are shown in Supplementary Table 1.

Functional State of Reactive Microglia and Astrocytes

Next, we sought to determine the cellular source of inflammation and performed colocalization of Iba1 or GFAP against inflammatory markers. Neither of the tested proinflammatory cytokines (IL-1β, TNF-α, and IL-10) and C3 (data not shown) nor polarization marker iNOS (Figure 6) was found in association with Iba1-*ir*. However, Iba1-*ir* cells colocalized with Arg1-*ir* and phagocytic marker CD68-*ir* at 7 and 21 dpi (Figure 6). A signal cooccurrence was observed at rod and amoeboid cells at 7 and 21 dpi, while only amoeboid $Iba1^+$ cells were abundantly labeled with eN/CD73 (Figure 6). The induction of the chemotaxis microglial marker $P2Y_{12}R$ was also observed at Iba1-*ir* cells at 7 dpi (Figure 6). Although a slight increase in the relative gene expression of $P2Y_{12}R$ was observed, $Iba1^+$ cells of amoeboid morphology did not colocalize with $P2Y_{12}R^+$ at 21 dpi (Figure 6). It is important to emphasize that ramified morphology of $Iba1^+$ cells (Figure 6) corresponds to Ctrl microglia as well as to $Iba1^+$ cells with the same morphology in the hippocampal areas distant from the site of neurodegeneration at both 7 and 21 dpi. Moreover, $P2X_7$-*ir* clearly labeled neurons in Ctrl hippocampi as well as at 7 dpi (Figure 6), while $P2X_7$-*ir* signal clearly overlapped with amoeboid microglia at 21 dpi. On the other hand, colocalization of $P2X_7R$ with GFAP-*ir* astrocytes could not be observed in Ctrls and investigated time points.

The lack of expression of proinflammatory cytokines and markers by Iba1-*ir* microglial cells, and clearly labeled $iNOS^+$ and $C3^+$ cells around $Iba1^+$ cells, prompted us to explore their astroglial expression (Figure 7). Except for neuronal TNF-α-*ir* at the site of neurodegeneration at 7 dpi, the signals that correspond to IL-1β, TNF-α, and IL-10 almost completely overlapped with GFAP-*ir* at 7 dpi and/or 21 dpi (Figure 7). At 7 dpi, iNOS- and C3-*ir* were also observed at neurons, while almost all GFAP-*ir* cells at the injured area expressed iNOS, nuclear factor-kB (NF-kB), and C3, suggesting that astrocytes were the major source of the inflammatory factors at the late stage of TMT-induced neurodegeneration. The fluorescence intensity of all investigated inflammatory markers was significantly increased at both 7 and 21 dpi (Figure 7).

Since astrocytic $P2Y_1R$ is involved in the regulation of several cytokines/chemokines expression (e.g., IL-6, and TNF-α) (Kuboyama et al., 2011), and $A_{2A}R$ upregulation in activated glial cells facilitates the release of cytokines (Paiva et al., 2019), we explore their localization. In addition, prolonged adenosine A_1R signaling and its cross-talk with $A_{2A}R$ might enhance $A_{2A}R$-mediated neurotoxicity in neurodegenerative disorders (Stockwell et al., 2017). Thus, massive induction of $P2Y_1R$ and $A_{2A}R$ was found on GFAP-*ir* and C3-*ir* astrocytes at 7 and 21 dpi, while A_1R shifted from neurons to GFAP-*ir* astrocytes at 7 dpi and fully colocalize with GFAP-*ir* at 21 dpi at the sites of neurodegeneration (mCA3 or CA1) (Figure 8). Neither one of the investigated receptors was not observed at $Iba1^+$ cells, suggesting the involvement of the purinoreceptors in the proinflammatory astrocyte phenotype after TMT intoxication.

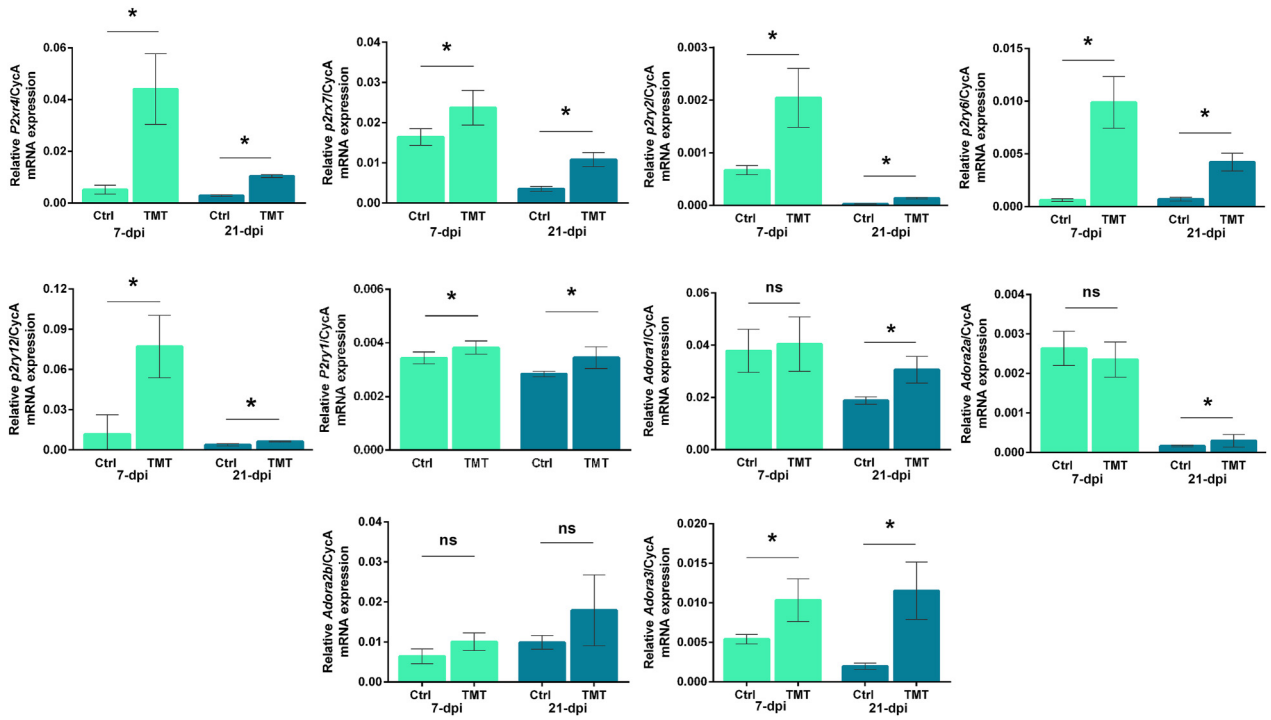

Figure 4. Purinoceptors gene expression in the hippocampal region after TMT exposure The abundances of transcripts coding for $P2X_4$, $P2X_7$, $P2Y_1R$, $P2Y_2R$, $P2Y_6R$, $P2Y_{12}R$, A_1R, $A_{2A}R$, $A_{2B}R$, and A_3R were assessed by RT-qPCR at 7 and 21 dpi. Bars represent mean mRNA expression of target gene relative to CycA ± SD. Significance shown inside the graphs: $*p < .05$ or less compared to age-match Ctrl.
Note. Ctrl = control; CycA = cyclophilin A; SD = standard deviation; RT-qPCR = quantitative reverse transcriptase-polymerase chain reaction; dpi = days post intoxication; mRNA = messenger RNA.

Discussion

The results of the present study corroborate the existing data on the spatiotemporal pattern of neurodegeneration and gliosis in the rat TMT model (Corvino et al., 2013, 2015; Haga et al., 2002; Latini et al., 2010; Little et al., 2012; Trabucco et al., 2009). As described and analyzed previously (Dragic et al., 2019b), reactive astrocytes (from day 2 post-TMT) were polarized toward the jeopardized regions, enclosing it and probably creating a protective glial barrier, keeping other regions from damage at the early stage of TMT-induced neurotoxicity (Dragic et al., 2019b). Microglial activation induced by TMT slightly lagged behind astrocyte reactivation, as observed earlier (Haga et al., 2002), and is manifested as a robust increase in the number of $Iba1^+$ cells due to migration or proliferation of resident microglia (Little et al., 2002). However, we observed that synaptic layers in the affected sectors became largely populated with *rod* $Iba1^+$ cells, occasionally found in a train formation at the early stage of neurodegeneration. Rod microglia are usually found at the early stages of neurodegenerative disorders in association with undamaged neurons and axons, and not in aggregation with other glial cells (Au & Ma, 2017; Zabel & Kirsch, 2013), which could be an indicator of their protective and reparative role (Boche et al., 2013). Rod cells may provide new cells and transform into amoeboid microglia (Tam & Ma, 2014). We also observed that injured neuronal cell layers of the hippocampal CA areas became sequentially infiltrated with $Iba1^+$ cells of amoeboid shape, particularly at the late stage of neurodegeneration induced by TMT.

As a marker of microglia (Almolda et al., 2013; Braun et al., 2000), NTPDase1/CD39 activity and expression were markedly upregulated in all Iba1-*ir* cells after TMT intoxication, irrespective of their shape and position. On the other hand, as the final and the rate-limiting enzyme in the extracellular degradation of ATP, eN/CD73 showed a selective switch from neuropil to amoeboid Iba1-*ir* cells, implicating that the differential induction might be an adaption to specific hippocampal microenvironment, that is, site of injury or specific function. The transition between functional states of reactive microglia is accompanied by the morphological transformation of the cells, and among the critical factors that trigger the transition are ATP, adenosine, vitamin E, IL-34, and chemokine fractalkine (Boche et al., 2013; Wollmer et al., 2001). Furthermore, NTPDase1/CD39 and eN/CD73 upregulation may represent a defense mechanism against excess levels of extracellular ATP originating from damaged cells (Braun et al., 2000; Burnstock, 2017). Thus, enhanced activity of NTPDase1/CD39 may contribute to the prevention of receptor desensitization on prolonged exposure to elevated ATP and prevent activated microglia from overstimulation by

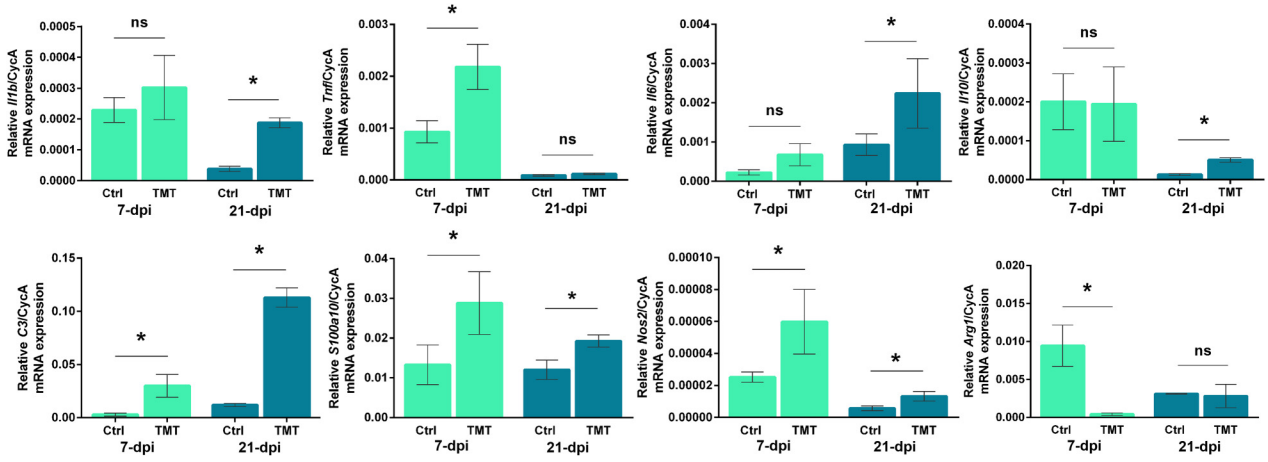

Figure 5. Proinflammatory status of the rat hippocampal region after TMT exposure The abundance of transcripts coding IL-1β, TNF-α, IL-6, IL-10, C3, S100a10, iNOS, and Arg1. Bars represent mean mRNA expression of target gene relative to CycA ± SD. Significance shown inside the graphs: *$p < .05$ or less compared to age-match Ctrl.
Note. Arg1 = arginase-1; CycA = cyclophilin A; IL-10 = interleukin-10; IL-1β = interleukin-1β; iNOS = inducible nitric oxide synthase; mRNA = messenger RNA; TMT = trimethyltin; TNF-α = tumor necrosis factor-α; SD = standard deviation.

ATP. The parallel eN/CD73 activity on amoeboid Iba1$^+$ cells probably facilitates the formation of adenosine that exerts neuro- and immunomodulatory actions (Di Virgilio et al., 2009; Illes et al., 2020). Furthermore, NTPDase1/CD39 and eN/CD73 not only catabolize extracellular ATP and provide adenosine but also function as clusters of differentiation and

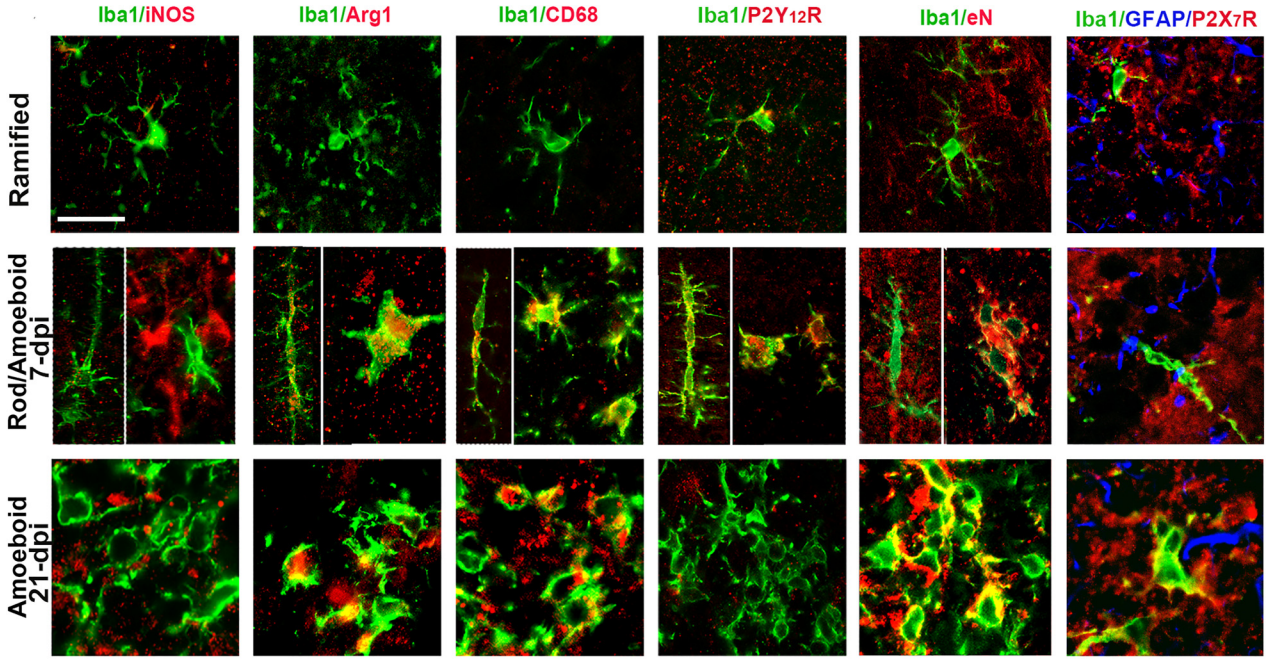

Figure 6. Assessment of the functional state of reactive microglia after TMT exposure. Ramified morphology of Iba1+cells corresponds to control microglia but also to ramified Iba1$^+$ cells in the hippocampal areas distant from the site of neurodegeneration at both 7 and 21 dpi. Double immunofluorescent staining of Iba1 and iNOS, Arg1, CD68, P2Y12 receptor (R), and eN/CD73, and triple immunofluorescent staining of Iba1, GFAP and P2X7R in the injured area 7 and 21 dpi, reveal Iba1-*ir* morphotypes that expressed Arg1-, CD68-, P2Y12-, P2X7- as well as eN-*ir*. Scale bar = 50 μm.
Note. Arg1 = arginase-1; dpi = days post intoxication; eN/CD73 = ecto-5′ nucleotidase; GFAP = glial fibrillary acidic protein; iNOS = inducible nitric oxide synthase; iNOS = inducible nitric oxide synthase; TMT = trimethyltin.

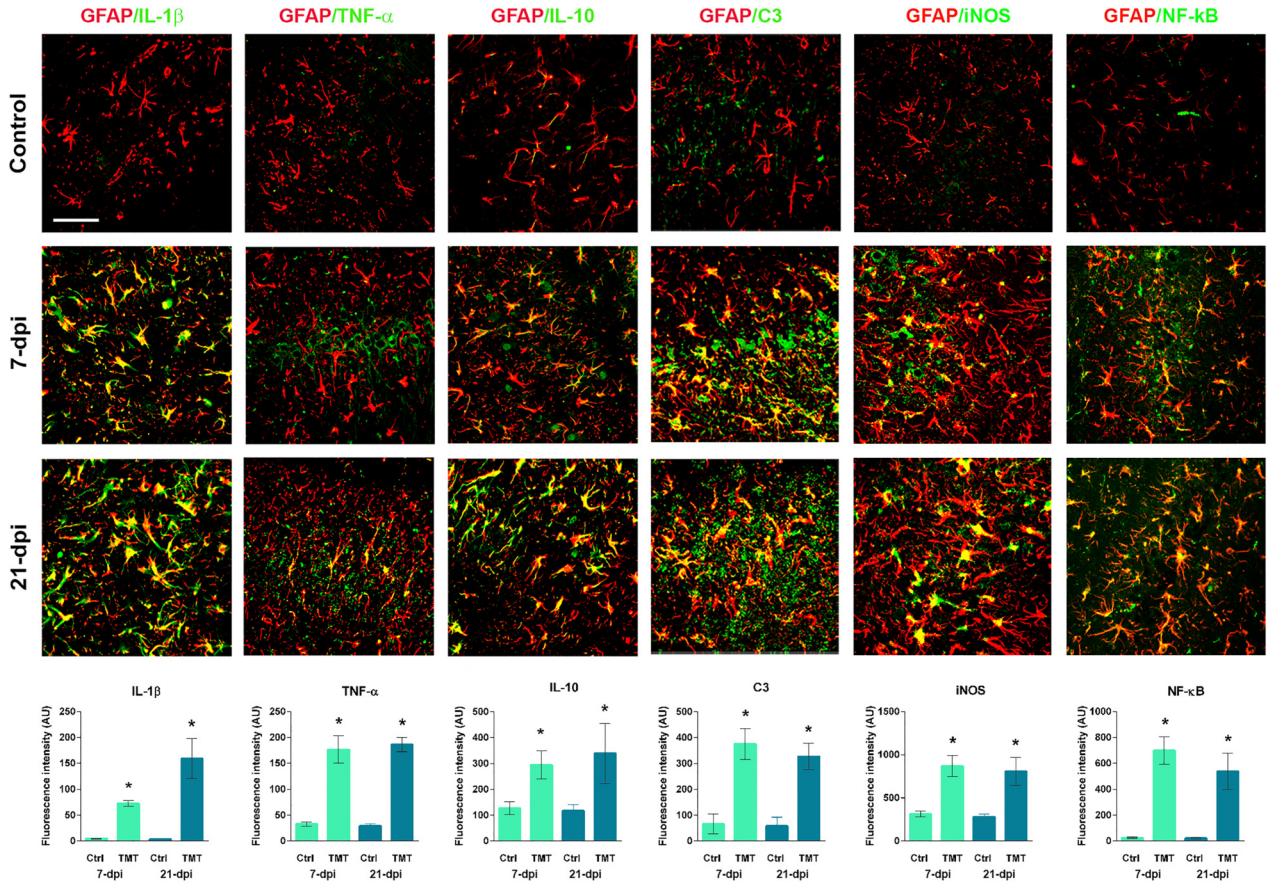

Figure 7. Assessment of the functional state of reactive astrocytes after TMT exposure. Double immunofluorescent staining of GFAP and IL-1β, TNF-α, IL-10, C3, iNOS and NF-kB and corresponding integrated fluorescence density expressed as AUs ± SEM in the injured CA area at 7 and 21 dpi. Significance shown inside the graphs: $*p < .05$ or less compared to age-match Ctrl.

Note. AU = arbitrary unit; Ctrl = control; dpi = days post intoxication; GFAP = glial fibrillary acidic protein; IL-10 = interleukin-10; IL-1β = interleukin-1β; iNOS = inducible nitric oxide synthase; NF-kB = nuclear factor-kB; SEM = standard error of the mean; TMT = trimethyltin; TNF-α = tumor necrosis factor α.

cell adhesion molecules, which regulate the adhesion and glial cell migration through specific interactions with extracellular matrix components (Koizumi et al., 2007).

Microglial cell migration and chemotaxis depend on purinergic signaling via P2 receptors (Illes et al., 2020; Koizumi et al., 2007), which also triggers their shift to amoeboid phenotype (Illes et al., 2020). Thus, we found an increase in relative gene expression of $P2Y_{12}R$ specifically at the early stage (7 dpi) of TMT-induced neurodegeneration. This receptor is activated by extracellular ATP released from damaged cells that trigger microglial processes extension and migration to the site of injury (Illes et al., 2020). Further, we found an increase in $P2X_4$ relative gene expression that may contribute to both migratory as well as secretory properties of microglia, and interacts with the $P2Y_{12}R$ in the regulation of chemotaxis (Illes et al., 2020). At this stage, an increase of $P2Y_6$-mRNA level was observed, a receptor upregulated when neurons become damaged and send diffusible uridine 5′-diphosphate (UDP) signals to microglia (Illes et al., 2020). Adenosine also affects extension and chemotaxis to the site of active neurodegeneration via $P2Y_{12}R/A_3R$ coactivation (Haynes et al., 2006; Ohsawa et al., 2012). The ADP-driven process extension was reversed to process retraction during proinflammatory condition coincident with $P2Y_{12}R$ protein downregulation (Orr et al., 2009), which we observed at the late stage of TMT-induced neurodegeneration. Additionally, $P2Y_6R$ stimulation blocks ATP-dependent migration of microglia, most likely by shifting its migratory phenotype to an amoeboid/phagocytic one (Bernier et al., 2013; Koizumi et al., 2007), and which upregulation persist at the late stage (21 dpi) of neurodegeneration. The mRNA levels of $P2X_7R$, the ATP-sensitive receptor predominantly localized on microglial cells in the brain (Illes et al., 2020), were also increased at both the early and the late stage of neurodegeneration.

Concerning the polarization state of microglia, our data showed that Iba1-*ir* cells coexpressed specific marker Arg1, and did not colocalize with proinflammatory

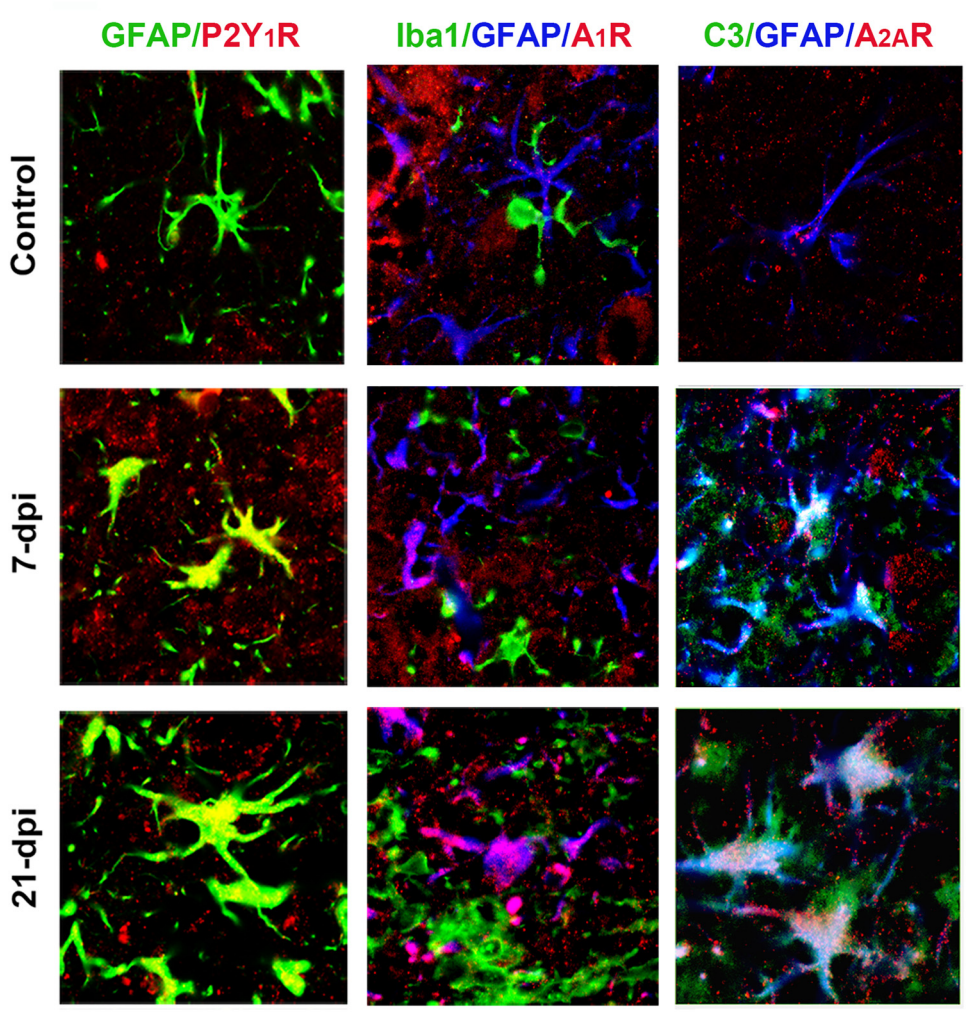

Figure 8. Association of P2Y1 and adenosine receptors with GFAP$^+$ astrocytes in the hippocampus after TMT exposure. Double IF reveals that GFAP-*ir* cells colocalized with $P2Y_1R$ in the injured hippocampal area at 7 and 21 dpi. Representative micrographs of triple IF staining of A_1R and markers of glial cells (Iba1 and GFAP) reveal neuronal A_1R staining in the Ctrl, colocalization with GFAP$^+$ cells at 7 dpi, and complete overlap of GFAP- and A_1R-*ir* at 21 dpi in the injured hippocampal area, without colocalization with Iba1-*ir* cells. Representative triple staining micrographs with C3, GFAP and $A_{2A}R$ reveal colocalization of all three signals in the injured hippocampal area at 7 and 21 dpi. Scale bar = 50 μm.

Note. GFAP = glial fibrillary acidic protein; TMT = trimethyltin; *ir* = immunoreactive; Ctrl = control; dpi = days post intoxication; IF = immunofluorescence.

markers iNOS, NF-kB, C3, and investigated proinflammatory cytokines, indicating that reactive microglial cells at the site of TMT-induced neurodegeneration were not a source of inflammatory molecules. The upregulation of NTPDase1/CD39 by reactive microglial cells was previously demonstrated in experimental autoimmune encephalomyelitis, where the induction of NTPDase1/CD39 tended to be associated with Arg1-*ir* and phagocytic marker CD68-*ir* microglial cells (Jakovljevic et al., 2019). Upregulation and specific localization of eN/CD73 on amoeboid Iba1$^+$ cells that were also associated with Arg1- and CD68-*ir* at the late stage of neurodegeneration induced by TMT support results that such eN/CD73 expression might promote macrophages/microglia to *phagocytic state* (Xu et al., 2018). In addition, $P2X_7$-*ir*, greatly localized on neurons at the early stage of neurodegeneration, colocalized with amoeboid Iba1-*ir* cells at the late stage of neurodegeneration. It is well known that $P2X_7R$ expression at amoeboid microglial cells modulates clearance of extracellular debris thus affecting their phagocytic role (Campagno & Mitchell, 2021). Given that CD39/CD73 tandem effectuate the whole cascade of extracellular ATP degradation, they might be taken as an "immunological switch" that leads to the antiinflammatory cell state (Antonioli et al., 2013), however, additional experiments are required to test this hypothesis.

According to the literature data (Little et al., 2002, 2012) early neurodegenerative response to TMT is not accompanied by increased gene expression of most proinflammatory cytokines. We found moderate induction of TNF-α in neurons at the early stage of TMT-induced neurodegeneration, while almost all $GFAP^+$ cells around damaged areas (CA1 and mCA3) were the source of IL-1β, TNF-α, and IL-10 particularly at the late stage of TMT-induced neurodegeneration, supporting in vitro results (Dragic et al., 2021) and studies that showed upregulation of other proinflammatory mediators at the later stages of TMT-induced neurodegeneration (Lattanzi et al., 2013; Liu et al., 2005; Morita et al., 2008). Furthermore, $P2X_7R$ is considered as a major driver of inflammation (Di Virgilio et al., 2017; Erb et al., 2019; Franke et al., 2012; Peterson et al., 2010), and we observed increased neuronal staining with $P2X_7R$ at both the early and the late stage of TMT-induced neurodegeneration. A wave of neurodegeneration induced by TMT might provide conditions for a sustained ATP release and prolonged $P2X_7R$ activation with the resulting postponed induction of IL-1β, together with TNF-α, and IL-6. Reactive astrocytes might initiate upregulation of $P2Y_2R$, as we observed after TMT intoxication, leading to a proinflammatory response (Peterson et al., 2010).

We have also observed that reactive astrocytes coexpressed iNOS, NF-kB, C3, and found increased expression of S100a10-mRNA. Taken together with the expression of main proinflammatory markers, it could be concluded that TMT-induced reactive astrogliosis exerts a complex molecular signature with the predominantly inflammatory phenotype (Escartin et al., 2021), mainly located around the sites of ongoing neurodegeneration. These proinflammatory astrocytes at the injured area also upregulate A_1R and $A_{2A}R$ receptors. In the hippocampus, adenosine exerts inhibitory function under physiological conditions due to the high expression of neuronal A_1R, modulating important processes such as learning and memory (Costenla et al., 2010; Stockwell et al., 2017). On the other hand, under pathological conditions, an increase of both mRNA and protein levels and aberrant signaling via hippocampal $A_{2A}R$ have been demonstrated to contribute to active neuroinflammation and cognitive deficits (Hu et al., 2016), both of which are seen in TMT-induced neurodegeneration (Geloso et al., 2011). Adenosine signaling via neuronal A_1R supports survival, exerts neuroprotective effects, and has anticonvulsive properties (Glass et al., 1996). Thus, the shift of A_1R immunoreactivity from neurons to astrocytes could render neurons vulnerable to secondary effects of TMT, such as seizures (Trabucco et al., 2009), while prolonged adenosine A_1R signaling and its cross-talk with $A_{2A}R$ might enhance $A_{2A}R$-mediated neurotoxicity in neurodegenerative disorders (Stockwell et al., 2017). Taken together with a concomitant increase of astrocytic $A_{2A}R$, these results could be put in perspective of potential formation of A_1R–$A_{2A}R$ heteromers, which are shown to contribute to dysregulation of glutamate homeostasis and favor excitotoxicity (Borroto-Escuela et al., 2018; Hou et al., 2020). A high amount of ATP released after TMT intoxication would be degraded by $Iba1^+/CD39^+/CD73^+$ cells thus producing high levels of adenosine around the sites of injury. Adenosine in such a microenvironment may activate astrocytic A_1R and $A_{2A}R$ supporting their proinflammatory phenotype (Nedeljkovic, 2019; Paiva et al., 2019; Popoli & Pepponi, 2012). Additional experiments are necessary to fully elucidate the role of adenosine in such a complex pathological environment. Induction of $P2Y_1R$ on reactive astrocytes further confirms their detrimental phenotype after TMT-induced neurotoxicity, since this receptor is also involved in the regulation of several cytokines/chemokines expression (Kuboyama et al., 2011), and causes astrocytic hyperactivity and dysfunction in an animal model of neurodegeneration (Delekate et al., 2014).

In summary, identification of expressional timeline of selected purinoreceptors and ectonucleotidases provides a framework for the reconstruction of their involvement in the initiation and progression of neurodegenerative events after TMT intoxication. This study suggests that proinflammatory astrocytes phenotype is possibly developed as a response to TMT intoxication. Increased availability of ligands such as ATP and adenosine coupled with a distinct set of activated glial purinergic repertoire ($P2X_7$, $A_{2A}R$, $P2Y_1$, and A_1R) and loss of homeostatic glial and neuronal purinergic pathways ($P2Y_{12}$ and A_1R) may shift purinergic signaling balance toward excitotoxicity and inflammation, thus ultimately favoring progression of pathological events. Targeting the upstream nucleotide metabolic pathway that controls adenosine production to modulate neural-immune interactions and neurodegeneration-related machinery represents a promising therapeutic strategy for intervening in disease progression.

Acknowledgments

The research was funded by the Ministry of Education, Science, and Technological Development of the Republic of Serbia Nos. 451-03-1/2021-16/14 –0902102 and 451-03-68/2020-14/200178. The authors thank Professor Jean Sevigny from the Faculté de Médecine, Université Laval, Quebec City, QC, Canada for a kind gift of rabbit anti-rat NTPDase1/CD39 (mN1-2C) and eN/CD73 (rNu-9L) antibodies used in this study. We would also like to thank our Dr. Ivana Bjelobaba, Institute for Biological Research "Siniša Stanković," National Institute of the Republic of Serbia, University of Belgrade, Belgrade, Serbia, for providing us with qPCR primers used in this study.

Author Contributions

All authors meet the International Committee of Medical Journal Editors (ICMJE) criteria for authorship for this article. I.G. conceived and directed the projects. M.D. and I.G. designed experiments and performed all histology, analyzed the data, and wrote the manuscript. N.M. performed qPCR experiments. M.A. was involved in confocal microscopy and image acquisition. N.N. was involved in data interpretation and wrote the manuscript. All authors had full access to all of the data in this study and take complete responsibility for the

integrity of the data and accuracy of the data analysis. All authors read, revised, and approved the final manuscript.

Data Availability Statement

The data that support the findings of this study are available from the corresponding author upon reasonable request.

Ethics Approval

The Ethical Committee approved all animal procedures for the Use of Laboratory Animals of "VINČA" Institute of Nuclear Sciences —National Institute of Republic of Serbia, University of Belgrade, Belgrade, Serbia, and animals were treated following the European Community Council Directive of 86/609/ EEC for animal experiment.

Declaration of Conflicting Interests

The authors declared no potential conflicts of interest with respect to the research, authorship, and/or publication of this article.

Funding

The authors disclosed receipt of the following financial support for the research, authorship, and/or publication of this article: This work was supported by the Ministarstvo Prosvete, Nauke i Tehnološkog Razvoja (grant numbers 451-03-68/2020-14/200178 and 451-03-1/2021-16/14 –0902102).

ORCID iD

Ivana Grković https://orcid.org/0000-0003-4476-7871

Supplemental Material

Supplemental material for this article is available online.

References

Almolda, B., Gonzalez, B., & Castellano, B. (2013). Microglia detection by enzymatic histochemistry. *Methods in Molecular Biology*, *1041*, 243–259. https://doi.org/10.1007/978-1-62703-520-0_22

Antonioli, L., Pacher, P., Vizi, E. S., & Haskó, G. (2013). CD39 and CD73 in immunity and inflammation. *Trends in Molecular Medicine*, *19*, 355–367. https://doi.org/10.1016/j.molmed.2013.03.005

Au, N. P. B., & Ma, C. H. E. (2017). Recent advances in the study of bipolar/rod-shaped microglia and their roles in neurodegeneration. *Frontiers in Aging Neuroscience*, *9*, 128. https://doi.org/10.3389/fnagi.2017.00128

Bernier, L. P., Ase, A. R., Boue-Grabot, E., & Séguéla, P. (2013). Inhibition of $P2X_4$ function by P2Y6 UDP receptors in microglia. *Glia*, *61*, 2038–2049. https://doi.org/10.1002/glia.22574

Boche, D., Perry, V. H., & Nicoll, J. A. (2013). Review: Activation patterns of microglia and their identification in the human brain. *Neuropathology and Applied Neurobiology*, *39*, 3–18. https://doi.org/10.1111/nan.12011

Borroto-Escuela, D. O., Hinz, S., Navarro, G., Rafael Franco, R., Müller, C.E., & Fuxe, K. (2018). Understanding the role of adenosine $A_{2A}R$ heteroreceptor complexes in neurodegeneration and neuroinflammation. *Frontiers in Neuroscience*, *12*, 43. https://doi.org/10.3389/fnins.2018.00043

Braun, N., Sevigny, J., Robson, S. C., Enjyoji, K., Guckelberger, O., Hammer, K., Di Virgilio, F., & Zimmermann, H. (2000). Assignment of ecto-nucleoside triphosphate diphosphohydrolase-1/cd39 expression to microglia and vasculature of the brain. *European Journal of Neuroscience*, *12*, 4357–4366.

Burnstock, G. (2017). Purinergic signalling: Therapeutic developments. *Frontiers in Pharmacology*, *8*, 661. https://doi.org/10.3389/fphar.2017.00661

Campagno, K. E., & Mitchell, C. H. (2021). The $P2X_7$ receptor in microglial cells modulates the endolysosomal axis, autophagy, and phagocytosis. *Frontiers in Cellular Neuroscience*, *15*, 645244. https://doi.org/10.3389/fncel.2021.645244

Chvojkova, M., Kubova, H., & Vales, K. (2021). Effects of dizocilpine, midazolam and their co-application on the trimethyltin (TMT)-induced rat model of cognitive deficit. *Brain Sciences*, *11*. https://doi.org/10.3390/brainsci11030400

Corvino, V., Di Maria, V., Marchese, E., Lattanzi, W., Biamonte, F., Michetti, F., & Geloso, M. C. (2015). Estrogen administration modulates hippocampal GABAergic subpopulations in the hippocampus of trimethyltin-treated rats. *Frontiers in Cellular Neuroscience*, *9*, 433. https://doi.org/10.3389/fncel.2015.00433

Corvino, V., Marchese, E., Michetti, F., & Geloso, M. C. (2013). Neuroprotective strategies in hippocampal neurodegeneration induced by the neurotoxicant trimethyltin. *Neurochemical Research*, *38*, 240–253. https://doi.org/10.1007/s11064-012-0932-9

Costenla, A. R., Cunha, R. A. de Mendonca, A. (2010). Caffeine, adenosine receptors, and synaptic plasticity. *Journal of Alzheimer's Disease*, *20*(Suppl 1), S25–S34. https://doi.org/10.3233/JAD-2010-091384

Delekate, A., Fuchtemeier, M., Schumacher, T., Ulbrich, C., Foddis, M., & Petzold, G.C. (2014). Metabotropic P2Y1 receptor signalling mediates astrocytic hyperactivity in vivo in an Alzheimer's Disease mouse model. *Nature Communications*, *5*, 5422. https://doi.org/10.1038/ncomms6422

Di Virgilio, F., Ceruti, S., Bramanti, P., & Abbracchio, M.P (2009). Purinergic signalling in inflammation of the central nervous system. *Trends in Neurosciences*, *32*, 79–87. https://doi.org/10.1016/j.tins.2008.11.003

Di Virgilio, F., Dal Ben, D., Sarti, A. C., Giuliani, A.L., & Falzoni, S. (2017). The $P2X_7$ receptor in infection and inflammation. *Immunity*, *47*, 15–31. https://doi.org/10.1016/j.immuni.2017.06.020

Dragic, M., Milicevic, K., Adzic, M., Stevanović, I., Ninković, M., Grković, I., Pavle Andjus, P., & Nedeljković, N. (2021). Trimethyltin increases intracellular Ca(2+) Via L-type voltage-gated calcium channels and promotes inflammatory phenotype in rat astrocytes in vitro. *Molecular Neurobiology*. 58(4):1792-1805 https://doi.org/10.1007/s12035-020-02273-x

Dragic, M., Zaric, M., Mitrovic, N., Nedeljković, N., & Grković, I. (2019a). Application of gray level Co-occurrence matrix analysis as a new method for enzyme histochemistry quantification. *Microscopy and Microanalysis*, *25*, 690–698. https://doi.org/10.1017/S1431927618016306

Dragic, M., Zaric, M., Mitrovic, N., Nedeljković. N., & Grković, I. (2019b). Two distinct hippocampal astrocyte morphotypes reveal subfield-different fate during neurodegeneration induced by trimethyltin intoxication. *Neuroscience*, *423*, 38–54. https://doi.org/10.1016/j.neuroscience.2019.10.022

Dunn, K. W., Kamocka, M. M., & McDonald, J. H. (2011). A practical guide to evaluating colocalization in biological microscopy. *American Journal of Physiology-Cell Physiology*, *300*, C723–C742. https://doi.org/10.1152/ajpcell.00462.2010

Erb, L., Woods, L. T., Khalafalla, M. G., & Weisman, G. A. (2019). Purinergic signaling in Alzheimer's disease. *Brain Research Bulletin*, *151*, 25–37. https://doi.org/10.1016/j.brainresbull.2018.10.014

Escartin, C., Galea, E. Lakatos, A., O'Callaghan, J. P., Petzold, G. C., Serrano-Pozo, A., Steinhäuser, C., Volterra, A., Carmignoto, G., Agarwal, A., Allen, N. J., Araque, A., Barbeito, L., Barzilai A., Bergles D. E., Bonvento G., Butt A. M., Chen W. T., Cohen-Salmon M., . . . Verkhratsky A. (2021). Reactive astrocyte nomenclature, definitions, and future directions. *Nature Neuroscience*, *24*, 312–325. https://doi.org/10.1038/s41593-020-00783-4

Ferraz da Silva, I., Freitas-Lima, L. C., Graceli, J. B., & Rodrigues, L. C. M. (2017). Organotins in neuronal damage, brain function, and behavior: A short review. *Frontiers in Endocrinology (Lausanne)*, *8*, 366. https://doi.org/10.3389/fendo.2017.00366

Franke, H., Verkhratsky, A., Burnstock, G., & Illes, P. (2012). Pathophysiology of astroglial purinergic signalling. *Purinergic Signalling*, *8*, 629–657. https://doi.org/10.1007/s11302-012-9300-0

Geloso, M. C., Corvino, V., & Michetti, F. (2011). Trimethyltin-induced hippocampal degeneration as a tool to investigate neurodegenerative processes. *Neurochemistry International*, *58*, 729–738. https://doi.org/10.1016/j.neuint.2011.03.009

Glass, M., Faull, R. L., Bullock, J. Y., Jansen, K., Mee, E. W., Walker, E. B., Synek, B. J., & Dragunow, M. (1996). Loss of A1 adenosine receptors in human temporal lobe epilepsy. *Brain Research*, *710*, 56–68. https://doi.org/10.1016/0006-8993(95)01313-X

Grkovic, I., Drakulic, D., Martinovic, J., & Mitrovic, N. (2019a). Role of ectonucleotidases in synapse formation during brain development: Physiological and pathological implications. *Current Neuropharmacology*, *17*, 84–98. https://doi.org/10.2174/1570159X15666170518151541

Grkovic, I., Mitrovic, N., Dragic, M., Adžić, M., Drakulić, D., & Nedeljković, N. (2019b). Spatial distribution and expression of ectonucleotidases in Rat hippocampus after removal of ovaries and estradiol replacement. *Molecular Neurobiology*, *56*, 1933–1945. https://doi.org/10.1007/s12035-018-1217-3

Haga, S., Haga, C., Aizawa, T., & Ikeda, K. (2002). Neuronal degeneration and glial cell-responses following trimethyltin intoxication in the rat. *Acta Neuropathologica*, *103*, 575–582. https://doi.org/10.1007/s00401-001-0505-5

Hasko, G., & Cronstein, B. (2013). Regulation of inflammation by adenosine. *Frontiers in Immunology*, *4*, 85. https://doi.org/10.3389/fimmu.2013.00085

Haynes, S. E., Hollopeter, G., Yang, G., Kurpius, D., Dailey, M. E., Gan, W. B., & Julius, D. (2006). The P2Y12 receptor regulates microglial activation by extracellular nucleotides. *Nature Neuroscience*, *9*, 1512–1519. https://doi.org/10.1038/nn1805

Hou, X., Li, Y., Huang, Y., Zhao, H., & Gui, L. (2020). Adenosine receptor A1–A2a heteromers regulate EAAT2 expression and glutamate uptake via YY1-induced repression of PPARgamma transcription. *PPAR Research*, *2020*, 2410264. https://doi.org/10.1155/2020/2410264

Hu, Q., Ren, X., Liu, Y., Li, Z., Zhang, L., Chen, X., He, C., & Chen, J. F. (2016). Aberrant adenosine A2A receptor signaling contributes to neurodegeneration and cognitive impairments in a mouse model of synucleinopathy. *Experimental Neurology*, *283*, 213–223. https://doi.org/10.1016/j.expneurol.2016.05.040

Illes, P., Rubini, P., Ulrich, H., Zhao, Y., & Tang, Y. (2020). Regulation of microglial functions by purinergic mechanisms in the healthy and diseased CNS. *Cells*, *9*:1108. https://doi.org/10.3390/cells9051108

Jakovljevic, M., Lavrnja, I., Bozic, I., Milosevic, A., Bjelobaba, I., Savic, D., Sévigny, J., Pekovic, S., Nedeljkovic, N., & Laketa, D. (2019). Induction of NTPDase1/CD39 by reactive microglia and macrophages is associated with the functional state during EAE. *Frontiers in Neuroscience*, *13*, 410. https://doi.org/10.3389/fnins.2019.00410

Koizumi, S., Shigemoto-Mogami, Y., Nasu-Tada, K., Shinozaki, Y., Ohsawa, K., Tsuda, M., Joshi, B. V., Jacobson, K. A., Kohsaka, S., & Inoue, K. (2007). UDP Acting at P2Y6 receptors is a mediator of microglial phagocytosis. *Nature*, *446*, 1091–1095. https://doi.org/10.1038/nature05704

Kotake, Y. (2012). Molecular mechanisms of environmental organotin toxicity in mammals. *Biological & Pharmaceutical Bulletin*, *35*, 1876–1880. https://doi.org/10.1248/bpb.b212017

Kuboyama, K., Harada, H., Tozaki-Saitoh, H., Tsuda, M., Ushijima, K., & Inoue, K. (2011). Astrocytic P2Y(1) receptor is involved in the regulation of cytokine/chemokine transcription and cerebral damage in a rat model of cerebral ischemia. *Journal of Cerebral Blood Flow & Metabolism*, *31*, 1930–1941. https://doi.org/10.1038/jcbfm.2011.49

Latini, L., Geloso, M. C., Corvino, V., Giannetti, S., Florenzano, F., Viscomi, M. T., Michetti, F., & Molinari, M. (2010). Trimethyltin intoxication up-regulates nitric oxide synthase in neurons and purinergic ionotropic receptor 2 in astrocytes in the hippocampus. *Journal of Neuroscience Research*, *88*, 500–509.

Lattanzi, W., Corvino, V., Di Maria, V., Michetti, F., & Geloso, M. C. (2013). Gene expression profiling as a tool to investigate the molecular machinery activated during hippocampal neurodegeneration induced by trimethyltin (TMT) administration. *International Journal of Molecular Sciences*, *14*, 16817–16835. https://doi.org/10.3390/ijms140816817

Lee, S., Yang, M., Kim, J., Kang, S., Kim, J., Kim, J. C., Jung, C., Shin, T., Kim, S. H., & Moon, C. (2016). Trimethyltin-induced hippocampal neurodegeneration: A mechanism-based review. *Brain Research Bulletin*, *125*, 187–199. https://doi.org/10.1016/j.brainresbull.2016.07.010

Liddelow, S. A.Barres, B. A. (2017). Reactive astrocytes: Production, function, and therapeutic potential. *Immunity*, *46*, 957–967. https://doi.org/10.1016/j.immuni.2017.06.006

Little, A. R., Benkovic, S. A., Miller, D. B., & O'Callaghan, J. P. (2002). Chemically induced neuronal damage and gliosis: Enhanced expression of the proinflammatory chemokine, monocyte chemoattractant protein (MCP)-1, without a corresponding increase in proinflammatory cytokines(1). *Neuroscience*, *115*, 307–320. https://doi.org/10.1016/S0306-4522(02)00359-7

Little, A. R., Miller, D. B., Li, S., Kashon, M. L., & O'Callaghan, J. P. (2012). Trimethyltin-induced neurotoxicity: Gene expression pathway analysis, q-RT-PCR and immunoblotting reveal early effects associated with hippocampal damage and gliosis. *Neurotoxicology and Teratology*, *34*, 72–82. https://doi.org/10.1016/j.ntt.2011.09.012

Liu, Y., Imai, H., Sadamatsu, M., Tsunashima, K., & Kato, N. (2005). Cytokines participate in neuronal death induced by trimethyltin in the rat hippocampus via type II glucocorticoid receptors. *Neuroscience Research*, *51*, 319–327. https://doi.org/10.1016/j.neures.2004.12.005

Matyash, M., Zabiegalov, O., Wendt, S., Matyash, V., & Kettenmann, H. (2017). The adenosine generating enzymes CD39/CD73 control microglial processes ramification in the mouse brain. *PLoS One*, *12*, e0175012. https://doi.org/10.1371/journal.pone.0175012

Mitrovic, N., Gusevac, I., Drakulic, D., Stanojlović, M., Zlatković, J., Sévigny, J., Horvat, A., Nedeljković, N., & Grković, I. (2016). Regional and sex-related differences in modulating effects of female sex steroids on ecto-5′-nucleotidase expression in the rat cerebral cortex and hippocampus. *General and Comparative Endocrinology*, *235*, 100–107. https://doi.org/10.1016/j.ygcen.2016.06.018

Mitrovic, N., Zaric, M., Drakulic, D., Martinović, J., Sévigny, J., Stanojlović, M., Nedeljković, N., & Grković, I. (2017). 17beta-estradiol-induced synaptic rearrangements are accompanied by altered ectonucleotidase activities in male rat hippocampal synaptosomes. *Journal of Molecular Neuroscience*, *61*, 412–422. https://doi.org/10.1007/s12031-016-0877-6

Morita, M., Imai, H., Liu, Y., Xu, X., Sadamatsu, M., Nakagami, R., Shirakawa, T., Nakano, K., Kita, Y., Yoshida, K., Tsunashima, K., & Kato, N. (2008). FK506-protective effects against trimethyltin neurotoxicity in rats: Hippocampal expression analyses reveal the involvement of periarterial osteopontin. *Neuroscience*, *153*, 1135–1145. https://doi.org/10.1016/j.neuroscience.2008.01.078

Nedeljkovic, N. (2019). Complex regulation of ecto-5′-nucleotidase/CD73 and A_{2A}R-mediated adenosine signaling at neurovascular unit: A link between acute and chronic neuroinflammation. *Pharmacological Research*, *144*, 99–115. https://doi.org/10.1016/j.phrs.2019.04.007

Ohsawa, K., Sanagi, T., Nakamura, Y., Suzuki, E., Inoue, K., & Kohsaka, S. A. (2012). Adenosine A3 receptor is involved in ADP-induced microglial process extension and migration. *Journal of Neurochemistry*, *121*, 217–227. https://doi.org/10.1111/j.1471-4159.2012.07693.x

Orr, A. G., Orr, A. L., Li, X. J., Gross, R. E., & Traynelis, S. F. (2009). Adenosine A(2A) receptor mediates microglial process retraction. *Nature Neuroscience*, *12*, 872–878. https://doi.org/10.1038/nn.2341

Paiva, I., Carvalho, K.Santos, P., Cellai, L., Pavlou, M. A. S., Jain, G., Gnad, T., Pfeifer, A., Vieau, D., Fischer, A., Buée, L., Outeiro, T. F., & Blum, D. (2019). A2a R-induced transcriptional deregulation in astrocytes: An in vitro study. *Glia*, *67*, 2329–2342. https://doi.org/10.1002/glia.23688

Peterson, T. S., Camden, J. M., Wang, Y., Seye, C. I., Wood, W. G. , Sun, G. Y., Erb, L., Petris, M. J., & Weisman, G. A. (2010). P2y2 nucleotide receptor-mediated responses in brain cells. *Molecular Neurobiology*, *41*, 356–366. https://doi.org/10.1007/s12035-010-8115-7

Pompili, E., Fabrizi, C., Fumagalli, L., & Fornai, F. (2020). Autophagy in trimethyltin-induced neurodegeneration. *Journal of Neural Transmission (Vienna)*, *127*, 987–998. https://doi.org/10.1007/s00702-020-02210-1

Popoli, P., & Pepponi, R. (2012). Potential therapeutic relevance of adenosine A2B and A2A receptors in the central nervous system. *Cns & Neurological Disorders Drug Targets*, *11*, 664–674. https://doi.org/10.2174/187152712803581100

Robson, S. C., Sevigny, J.., & Zimmermann, H. (2006). The E-NTPDase family of ectonucleotidases: Structure function relationships and pathophysiological significance. *Purinergic Signalling*, *2*, 409–430. https://doi.org/10.1007/s11302-006-9003-5

Sperlagh, B., & Illes, P. (2007). Purinergic modulation of microglial cell activation. *Purinergic Signalling*, *3*, 117–127. https://doi.org/10.1007/s11302-006-9043-x

Stockwell, J., Jakova, E., & Cayabyab, F. S. (2017). Adenosine A1 and A2A receptors in the brain: Current research and their role in neurodegeneration. *Molecules*, *22*(4), 676. https://doi.org/10.3390/molecules22040676

Tam, W. Y.Ma, C. H. (2014). Bipolar/rod-shaped microglia are proliferating microglia with distinct M1/M2 phenotypes. *Scientific Reports*, *4*, 7279. https://doi.org/10.1038/srep07279

Trabucco, A., Di Pietro, P., Nori, S. L., Fulceri, F., Fumagalli, L., Paparelli, A., & Fornai, F. (2009). Methylated tin toxicity a reappraisal using rodents models. *Archives Italiennes de Biologie*, *147*, 141–153. PMID: 20162863.

Verkhratsky, A., Parpura, V., Pekna, M., Pekny, M., & Sofroniew, M. (2014). Glia in the pathogenesis of neurodegenerative diseases. *Biochemical Society Transactions*, *42*, 1291–1301. https://doi.org/10.1042/BST20140107

Wollmer, M. A., Lucius, R., Wilms, H., Held-Feindt, J., Sievers, J., & Mentlein, R. (2001). ATP And adenosine induce ramification of microglia in vitro. *Journal of Neuroimmunology*, *115*, 19–27. https://doi.org/10.1016/S0165-5728(01)00257-0

Xu, S., Zhu, W., Shao, M., Zhang, F., Guo, J., Xu, H., Jiang, J., Ma, X., Xia, X., Zhi, X., Zhou, P., & Lu, F. (2018). Ecto-5′-nucleotidase (CD73) attenuates inflammation after spinal cord injury by promoting macrophages/microglia M2 polarization in mice. *Journal of Neuroinflammation*, *15*, 155. https://doi.org/10.1186/s12974-018-1183-8

Ye, M., Han, B. H., Kim, J. S., Kim, K., & Shim, I. (2020). Neuroprotective effect of bean phosphatidylserine on TMT-induced memory deficits in a rat model. *International Journal of Molecular Sciences*, *21*(14), 4901. https://doi.org/10.3390/ijms21144901

Yegambaram, M., Manivannan, B., Beach, T. G., & Halden, R. U. (2015). Role of environmental contaminants in the etiology of Alzheimer's disease: A review. *Current Alzheimer Research*, *12*, 116–146. https://doi.org/10.2174/1567205012666150204121719

Zabel, M. K., & Kirsch, W. M. (2013). From development to dysfunction: Microglia and the complement cascade in CNS homeostasis. *Ageing Research Reviews*, *12*, 749–756. https://doi.org/10.1016/j.arr.2013.02.001

Zimmermann, H., Zebisch, M., & Strater, N. (2012). Cellular function and molecular structure of ecto-nucleotidases. *Purinergic Signalling*, *8*, 437–502. https://doi.org/10.1007/s11302-012-9309-4